Copyright

by

Tyler Don-Michel Elko-Hansen

2014

The Dissertation Committee for Tyler Don-Michel Elko-Hansen Certifies that this is the approved version of the following dissertation:

Surface Chemistry Considerations for Enhanced Vapor Deposition of Metals

Committee:

John G. Ekerdt, Supervisor

Gyeong S. Hwang

Brian A. Korgel

Charles B. Mullins

Richard A. Jones

Surface Chemistry Considerations for Enhanced Vapor Deposition of Metals

by

Tyler Don-Michel Elko-Hansen, B.S. ChE

Dissertation

Presented to the Faculty of the Graduate School of

The University of Texas at Austin

in Partial Fulfillment

of the Requirements

for the Degree of

Doctor of Philosophy

The University of Texas at Austin

May 2014

Dedication

To my loved ones, family and friends.

Acknowledgements

My work at The University of Texas Austin would not have been possible or enjoyable without the help and friendship of so many people. First and foremost I would like to thank my adviser Dr. John G. Ekerdt. Dr. Ekerdt is never too busy to lend an ear to a challenge or give advice for research or personal challenges. He has taught me many things and I can only hope that I can lead as well as he does someday. But even with a great mentor, my colleagues have made my experience a lasting memory. I would especially like to thank Dr. Blair Cox, Dr. Joe McCrate, Martin (DJ) McDaniel, James Knight, Thong Ngo, Paul Abel, Kyle Klavetter, Alex Rettie, Butch Cunningham, Jim Smitherman and Sonali Chopra for their ongoing support and valuable advice and friendship. I would also like to thank the following Ekerdt group colleagues who have offered support and advice: Wen Liao, Dr. Lucas Henderson, Brad Leonhardt, Daniel Bost, Dr. Tuo Wang, and Dr. Songyan Jia.

I would also like to thank Kevin Haynes, Eddie Ibarra, and T Stockman who always helped me get things done, especially at the last minute. The Chemical Engineering Department support staff as a whole has been very helpful throughout my PhD studies and deserves recognition.

Further, I would like to thank Dr. Jeanette Roberts and Dr. Scott Clendenning for their time and guidance during this project and Intel for the funding that made it all possible.

Finally I thank my friends and family from the bottom of my heart for being so good to me throughout my life and for being a constant reminder to me of those things that are most important.

Surface Chemistry Considerations for Enhanced Vapor Deposition of Metals

Tyler Don-Michel Elko-Hansen, Ph.D.

The University of Texas at Austin, 2014

Supervisor: John G. Ekerdt

Electrolessly deposited CoWP capping layers have been demonstrated to effectively reduce electromigration of Cu at the interconnect/dielectric-barrier cap interface while reducing resistivity relative to SiCN. However, as device dimensions scale, the need for alternative methods for the selective deposition of sub-5 nm, ultrathin, conformal Co capping layers is apparent. To develop methods for area-selective atomic layer deposition (AS-ALD) of Co caps for next-generation Cu interconnects, the ALD behavior of bis(N-tert-butyl-N'-ethylpropionamidinato) cobalt(II) (CoAMD) is evaluated on Cu, SiO_2, and a porous low-k (k ~2.6) dielectric, CDO. The first and second ALD half reactions of CoAMD on the respective substrates is evaluated with H_2 coreactant by adsorbing the precursor on the substrates under ALD cycling conditions at 265 °C with and without coreactant exposure. The adsorption studies indicate that CoAMD preferentially deposits most on Cu and least on CDO. Further, CoAMD, like other amidinate precursors, readily dissociates on the Cu transition metal surface but the ultimate per-cycle coverage is self-limited by the slow desorption of amidinate ligands and fragments from the Cu surface. Co films deposited by ALD from CoAMD on Cu at 265 °C indicate that Co burrows into the lower energy Cu surface as the film grows in order to reduce the free

surface energy. The Cu remains as a surfactant-like layer on the topmost Co surface up to film thicknesses of at least 16 nm. Moreover, considerable intermixing at the Co/Cu interface and Cu concentration several nm into the Co films are observed indicating high surface mobility of the two materials and Cu diffusion at polycrystalline Co grain boundaries. Finally, employing low-tempurature ALD and selectively passivating the dielectric surfaces with OH targeting passivants leads to enhanced selectivity of CoAMD for deposition on Cu versus SiO_2 and CDO. Depositing Co from CoAMD on Cu and CDO at 165 °C after 500 kTorr-s exposure to trimethylchlorosilane at 50 °C leads to a 30:1 preference for Co accumulation on Cu, a twelve times improvement compared to deposition on cleaned Cu and CDO at 265 °C.

Table of Contents

List of Figures x

INTRODUCTION **1**

I.1 Background 1

I.2 Electromigration 4

Cu EM Reduction 5

I.3 Film Growth and Chemical Methods for Area-Selective ALD 6

Area-selective ALD 8

BEOL Materials – Surface Chemistry Considerations 9

I.4 Objectives and Overview of Chapters 10

Additional Research 12

I.5 References 13

SECTION 1: CHEMICAL SELECTIVITY IN ATOMIC LAYER DEPOSITION OF COBALT CAPPING LAYERS **16**

Chapter 1: XPS investigation of the atomic layer deposition half reactions of bis(N-tert-butyl-N'-ethylpropionamidinato) cobalt(II) 16

1.1 Introduction 16

1.2 Experimental Section 18

1.3 Results 21

1.4 Discussion 25

1.5 Conclusions 28

1.6 References 29

Chapter 2: Interdiffusion and diffusive stabilization of cobalt by copper during atomic layer deposition from bis(N-tert-butyl-N'-ethylpropionamidinato) cobalt(II)31

2.1 Introduction 31

2.2 Experimental Section 32

2.3 Results and Discussion 35

2.4 Conclusions 42

2.5 References 43

Chapter 3: Selectivity-enhanced Atomic Layer Deposition of Co on Cu relative to SiO_2 and Carbon Doped Oxide Dielectrics....45
3.1 Introduction....45
3.2 Experimental Methods....46
3.3 Results and Discussion....48
3.4 Conclusions....55
3.5 References....56
Chapter 4: Summary....58
4.1 Conclusions....58
4.2 Recommendations for Future Work....59
4.6 References....62
SECTION 2: HETEROATOM ENHANCEMENT OF HOPG FOR ENHANCED PARTICLE NUCLEATION AND STABILIZATION **63**
Chapter 5: Enhanced Nucleation of Pt Particles on Boron-Treated Highly Oriented Pyrolytic Graphite via Chemical Vapor Deposition....63
5.1 Introduction....63
5.2 Experimental Methods....64
5.3 Results....66
5.4 Discussion....71
5.5 References....74
References....76
Vita 84

List of Figures

Figure I.1. Cross sectional SEM of 65 nm node metallization scheme. Darkest regions are Cu interconnects (intralevel connections) and vias (interlevel connections). Adapted from [7]. 2

Figure I.2. Concepts of pitch and node displayed on 45 nm-node Cu interconnects with low-k ILD. 3

Figure I.3. Example of EM-induced void failure (taken from [1]). 4

Figure I.4. EM Lifetime improvements versus resistance increases of various EM resistance solutions [3]..6

Figure I.5. Surface processes of adsorbate molecules. Adapted from [22], p. 147. 7

Figure I.6. Growth modes with surface energy considerations. γAB is the interfacial energy between the substrate B and the depositing film A. (a) represents Volmer-Weber or island growth, (b) Stranski-Krastanov or layer plus island, and (c) Frank-van der Merwe or layer by layer growth. (adapted from [22], p. 146)..8

Figure 1.1. ALD and analysis chamber. 19

Figure 1.2. Co 2*p* XP spectra of 3x2s CoAMD cycles on the respective substrates. All signals have been normalized with background subtraction (Shirley type). The Co signal intensity on Cu is reduced by one order of magnitude...20

Figure 1.3. Co 2*p* XP spectrum following a 1×4s-no-H_2 CoAMD exposure on SiO_2 at 100 °C. 21

Figure 1.4. Co 2*p* XP spectra from adsorption cycling on each substrate. The spectra indicate oxidized Co formed on SiO_2 and CDO and reduced Co formed on Cu, with or without H_2 exposure...22

Figure 1.5. 3×2s CoAMD adsorption on Cu at different temperatues. Co 2$p_{3/2}$ signals indicate reduced Co^0 (778.3eV) for all tested substrate temperatures.24
Figure 1.6. Residual C 1*s* and N 1*s* spectra on Cu after 1 or 3 ALD cycles and after one CoAMD half-cycle. N is present in small amounts. N 1*s* signals overlap but are offset deliberately for clarity. 24
Figure 1.7. One possible dissociative adsorption process of CoAMD on Cu during ALD cycling is depicted (the Ar purge after the H_2 exposure in the second half reaction is not shown). Circles represent Co and triangles represent amidinate ligands and fragments from the CoAMD precursor while the black line represents the Cu surface. 25
Figure 2.1**.** Plan-view SEM images of (A) 250, (B) 500, (C) 1000, and (D) 3000 cycle ALD depositions of CoAMD on Cu at 265 °C. The calibrated Co:Cu atomic ratio detected in XPS is listed in the upper right-hand corner of each figure. 36
Figure 2.2. Cross-sectional TEM images and surface topography renderings from AFM of (A) 1000 cycle and (B) 3000 cycle ALD of CoAMD on Cu at 265 °C. 37
Figure 2.3. ToF-SIMS depth profiles of 1000 cyc Co film: (A) and (C), and 3000 cycle Co film: (B) and (D). Adv. Matl. refers to adventitious material accumulated on the substrate during sample storage and after air transfer for analysis and was not present *in situ* following deposition. 38

Figure 2.4. As deposited Co (top) and Cu (bottom) 2*p* X-ray photoelectron spectra from a 16 nm (3000 ALD cycle from CoAMD) Co film on Cu substrate. The reduced Co^0 and Cu^0 positions are depicted by arrows at the $2p_{3/2}$ peaks, 778.3 eV and 932.7 eV, respectively. Some Cu signal is still apparent in XPS after Co deposition as indicated by the Cu 2*p* inset.39

Figure 2.5. Growth mode of Co films on Cu by ALD from CoAMD. 40

Figure 2.6. XRD data from Co films on Cu. (A) depicts the raw signal for a blank Cu substrate, 300 nm on Si, a 5 nm, 1000 ALD cycle Co film from CoAMD deposited at T_s: 265 °C, and a molecular beam epitaxy-deposited Co film on the same Cu substrate held at T_s: 265 °C. (B) depicts the inset from (A), boxed in red, and highlights the relevant XRD signals for the Co films. The fcc (111) signal may include information from Cu and Co from which the Co signal cannot be isolated. Further, hcp (100) and hcp (101) Co signals are not observed after ALD or MBE but are often indiscernible from the signal noise in sub-40 nm films [24]. A faint fcc (200) signal is apparent for the MBE sample. 41

Figure 3.1. Schematic for OH targeting passivation scheme. 49

Figure 3.2. XPS measured Co atomic percentages accumulated after 3×2s adsorption of CoAMD at 265 °C on passivant treated Cu, SiO_2, and CDO substrates. Co accumulation is normalized for each substrate relative to their respective Co accumulation with no surface passivation. Passivant treatments are listed in the figure legend. 50

Figure 3.3. Co accumulation after 250 ALD-cycle deposition of CoAMD at 265 °C on passivant treated Cu, SiO_2, and CDO substrates. Co accumulation is normalized for each substrate relative to their respective Co accumulation with no surface passivation. Passivant treatments are listed in the figure legend. 51

Figure 3.4. Co 2p XP spectra of Co accumulation after 250 ALD-cycle deposition of CoAMD at 265 °C on inert (A) polyimide and (B) Teflon surfaces.52

Figure 3.5. XPS derived Co atomic percentage accumulation on untreated Cu and CDO after 50 ALD cycles of CoAMD with H_2 at various temperatures. 53

Figure 3.6. Cross-sectional TEM images of Co accumulation on TMCS (50 kTorr-s at 50 °C) treated, acetic acid etched LSW substrates. (A) 500 cycle and (B) 1000 cycle Co ALD at 165 °C. 55

Figure 5.1. XP spectra of B 1s signal (BE 189.4 eV) in HOPG that underwent 12 L B2D6 exposure (——) and no exposure (• • • •) 67

Figure 5.2. Possible structures for B enhanced Pt binding sites where Pt atoms are blue, B atoms orange, and C grey. A) represents pyridine-like bond structure and B) represents Pt bridging from B to α-C. 68

Figure 5.3. SEM of Pt coverage after 5 min Pt synthesis. Left to Right: Pt on HOPG, Pt on AHOPG, Pt on BHOPG..69

Figure 5.4. SEM of Pt coverage after 30 min Pt synthesis. Left to Right: Pt on HOPG, Pt on AHOPG, Pt on BHOPG..69

Figure 5.5. SEM images from thermal stability study – 30 min Pt deposition on BHOPG. Left to Right: unmodified Pt on BHOPG, annealed to 300 °C, annealed to 500 °C. 70

Figure 5.6. Particle density vs. boron exposure. 71

INTRODUCTION

I.1 BACKGROUND

In efforts to maintain the profitability of integrated circuit (IC) devices and improve their performance, device features must decrease in size. However, the scaling of microelectronics produces many materials and manufacturing challenges for back end of line (BEOL) processes. The BEOL comprises the Cu and dielectric metallization structure that allows for power and signal transfer to and from the devices. Device scaling has led to premature device failure due to Cu electromigration (EM) [1,2]. This research addresses methods to reduce the effect of EM in BEOL Cu interconnects.

BEOL interconnects comprise multiple layers of intra- and interlevel Cu connections (interconnects and vias, respectively, see Figure I.1) separated from one another by interlayer dielectric (ILD) material. The industry defines technology nodes specifying the benchmark size of the smallest device dimension, *i.e.*, node denotes the half-pitch of a metallization layer (see Figure I.2). Each technology node reduces the size of the Cu interconnect lines that comprise the BEOL structure. Today, IC performance is limited by resistance (R) capacitive (C) delays in the BEOL metallization structure [3,4]. Given interconnect lines of resistivity (ρ), width (W), thickness (T), and length (L), and ILD material with dielectric constant (k), we can approximate the RC delay by the following:

$$R = \frac{\rho L}{WT} \tag{I.1}$$

$$C = 2\,kL\left(\frac{T}{W} + \frac{W}{T}\right) = 2(C_L + C_V) \tag{I.2}$$

$$RC = 2\,\rho\,kL^2\left(\frac{1}{W^2} + \frac{1}{T^2}\right) \tag{I.3}$$

where we assume the dielectric thickness above and below the interconnect is equal to T and that the dielectric width next to the interconnect is also W and C_L and C_V represent the intralevel and interlevel capacitance between interconnect lines. The dielectric constant k is an effective dielectric constant that accounts for the different dielectric materials used at the various metallization levels from M1 (connected to the active device) to the final metallization level. Six levels of interconnects, M1-M6, are depicted in Figure I.1 though many ICs now have around nine metallization layers, M9, depending on their application [3,5,6]. From equations I.1-I.3, very long interconnect lengths and decreases in line width and thickness contribute to the RC delay. For this reason, continued IC scaling dictates that ρ and k must be kept as low as possible.

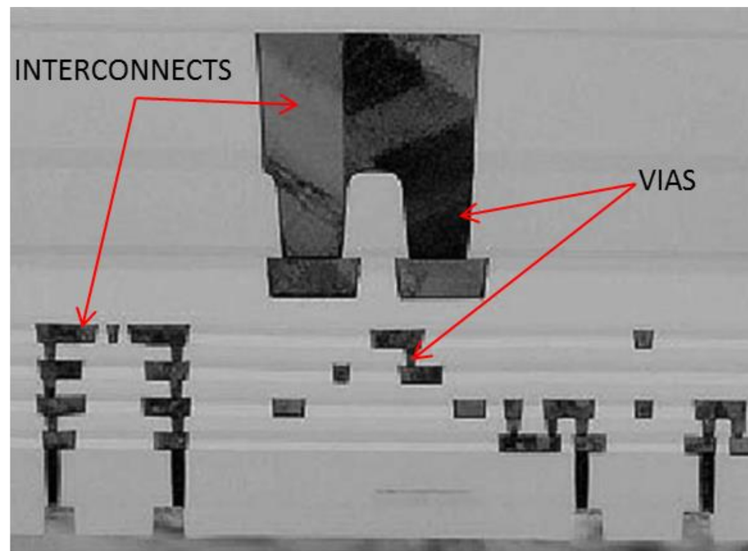

Figure I.1. Cross sectional SEM of 65 nm node metallization scheme. Darkest regions are Cu interconnects (intralevel connections) and vias (interlevel connections). Adapted from [7].

However, scaling also introduces considerable durability challenges for IC design. In particular, low-k dielectric materials present new materials constraints that were not a challenge for SiO_2. Low-k dielectrics are necessary to mitigate resistance-capacitive (RC) delay increases in BEOL structures due to capacitance between interconnects, signal cross-talk, and resistivity increases associated with Cu/dielectric interfaces [4–6]. SiO_2 has k ~4.0. By comparison, low-k dielectrics are expected to have k ranging from 2.5 to 3.0 for 2014 and 2015 shipments and k as low as 1.65 by 2025 [3]. While organosilica glasses (OSG), in which Si-O terminations are replaced in part by –H or $–CH_3$, achieve k ~2.7-3.0, achieving $k < 2.5$ generally requires some degree of porosity as $k_{air} = 1.0$ [3,7,8]. Porous media generally sacrifice mechanical strength such that too much porosity may lead to device fracture during packaging [3,10]. For the 45 nm technology node, the dielectric has k ~2.5 and may be an OSG with many $Si-CH_3$ terminations and a small degree of porosity. Such a dielectric is the model ILD for this work and is denoted CDO for carbon-doped oxide.

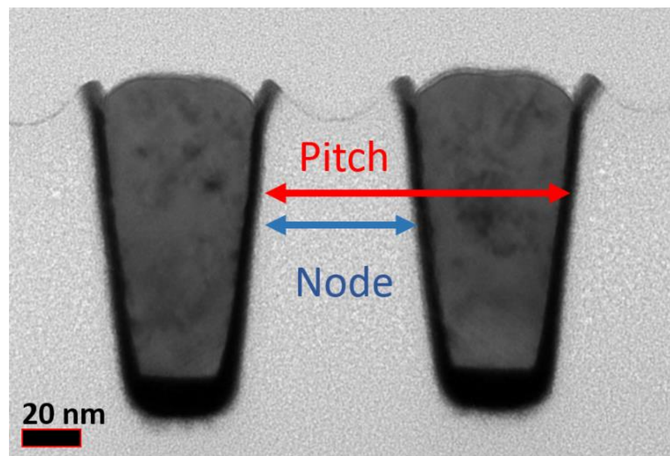

Figure I.2. Concepts of pitch and node displayed on 45 nm-node Cu interconnects with low-k ILD.

Another considerable challenge affecting ICs is premature failure due to copper EM. EM concerns have existed in IC fabrication for many generations and plagued the original Al interconnects. Due to the strong failure mode of Al interconnects by void formation at grain boundaries, they were supplanted by Cu interconnects that exhibited more resistance to EM and a different dominant failure mode: EM at the dielectric-barrier interface [11]. The Si(C)N dielectric barrier cap serves to protect the Cu metallization lines from oxidation during the growth of the next highest dielectric layer but also to help resist Cu EM. However, it has been demonstrated that the Cu/Si(C)N is an accelerated Cu diffusion path and beginning with the 90 nm node, new solutions to reduce Cu EM have been necessary [3,9].

I.2 ELECTROMIGRATION

Electromigration is the mechanism by which momentum from flowing electrons is conferred on the metal through which it passes, leading to self-diffusion of the metal atoms in the direction of the electron flow. Over time the EM of Cu can result in a loss of connection in an interconnect line due to void failure (Figure I.3). For many technology

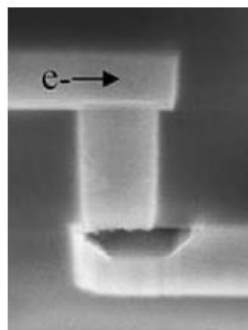

Figure I.3. Example of EM-induced void failure (taken from [1]).

nodes, the fastest EM pathway for Cu interconnects has been at the Cu-Si(C)N dielectric barrier interface. This is due in part to the relatively poor adhesion between the Cu and Si(C)N layers relative to metal capping layers [13].

Cu EM Reduction

Various methods for reducing Cu EM have been developed. In particular, Cu interconnect alloying and capping have been widely investigated to reduce Cu EM [1,4–8]. Silicidation of the Cu surface before application of the Si(C)N dielectric barrier may yield 50% improvement in EM lifetime with about 3% resistance increase [17,18]. Alloying with Al or Mn are the most common options with concentrations of only 0.3% yielding up to more than one-hundred fold improvements in device lifetime, though the alloyed interconnects exhibit nearly four-fold greater resistance than CoWP caps [3]. The resistance increase results in greater parasitic power loss and RC delay reducing the maximum computing speed of an IC [3,19]. Figure I.4 depicts a comparison of the interconnect lifetime benefits of various EM solutions as they relate to their increase in interconnect resistance relative to untreated Cu interconnects [3].

Capping layers are generally preferred to Cu alloying due to the increased interconnect resistivity associated with alloying [3]. The Si(C)N dielectric barrier cap itself reduces Cu EM relative to uncapped Cu lines. CuSiN layers exhibit two times or more resistivity increase than CoWP caps though they have shown similar EM lifetimes for which one-hundred fold improvements are common in the literature [3,16]. To minimize RC delay and maximize device lifetime, Co capping layers represent the best candidate for Cu EM reduction as IC scaling continues.

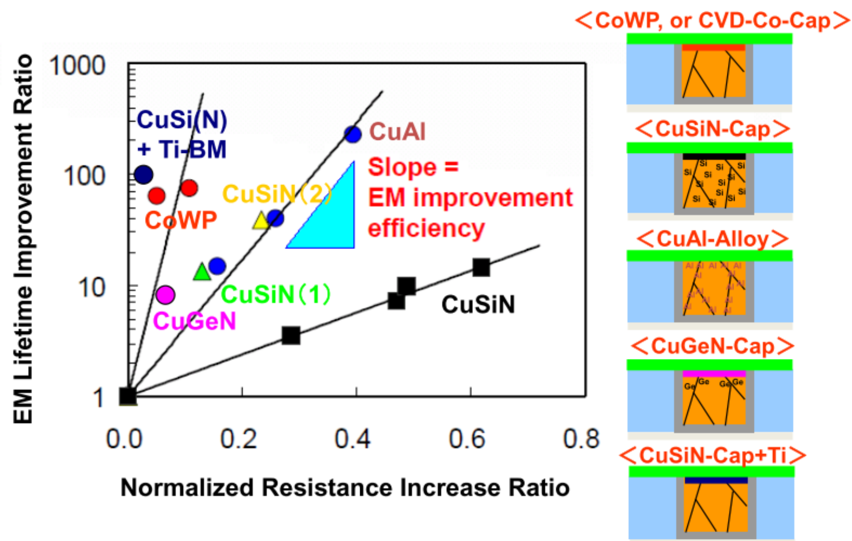

Figure I.4. EM Lifetime improvements versus resistance increases of various EM resistance solutions [3].

Considering CoWP as an EM solution includes determining how best to implement the films in a manufacturing process. As the current benchmark, CoWP may be selectively deposited by electroless deposition [17,18]. However, to avoid ILD contamination by the plating bath and to increase control of the deposition of ultrathin EM barrier caps (< 5 nm) much interest exists to develop selective atomic layer deposition (ALD) and chemical vapor deposition (CVD) processes [3,11]. Selective ALD processes are optimal as they can be tuned for surface selectivity based on surface chemistry and deposit highly-controllable, conformal films. In this work, methods to enable the area-selective ALD of Co capping layers from bis(N-tert-butyl-N'-ethylpropionamidinato) cobalt(II) are investigated.

I.3 Film Growth and Chemical Methods for Area-Selective ALD

The deposition of thin films concerns thermodynamic and kinetic relationships. It begins with an adsorption event during which precursor adsorbate atoms impinge on the substrate surface. Once on the surface they may (i) desorb, (ii) diffuse, (iii) bond to surface

"defect" sites, (iv) interdiffuse with the substrate material, (v) coalesce with adjacent adsorbate molecules and nucleate an overlayer island, or any combination of (ii) – (v) (Figure I.5).

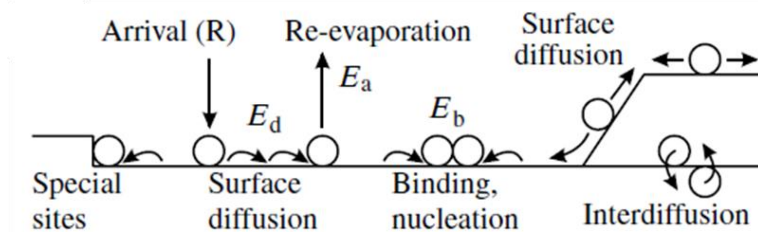

Figure I.5. Surface processes of adsorbate molecules. Adapted from [22], p. 147.

Of particular importance to the film structure of an overlayer on a homogenous substrate is the discussion of surface energies [22]. We can consider the interaction of a depositing material A on a substrate surface B by examining the respective surface energies γ_A and γ_B and their interfacial energy γ_{AB}. Figure I.6 depicts the common growth modes and how they correspond to the respective surface and interfacial energies. If $\gamma_A + \gamma_{AB} < \gamma_B$ then layer by layer, or Frank-van der Merwe, growth ensues (Fig I.6a). The converse of this being a substrate with lower surface energy than growing interface and film yields island or Volmer-Weber growth (Fig I.6c). A third case exists that is fairly common in heteroepitaxial film deposition for which the depositing film first forms layers but as the film thickens islands form on top of the conforming film. This mode is called Stranski-Krastanov (SK) growth and may be explained by considering that the initial conformal film layers are forced to match the substrate crystalline structure, the mismatch between the two materials causes strain in the growing film which increases until the strain must be reconciled and islands result (Fig I.6b) [22].

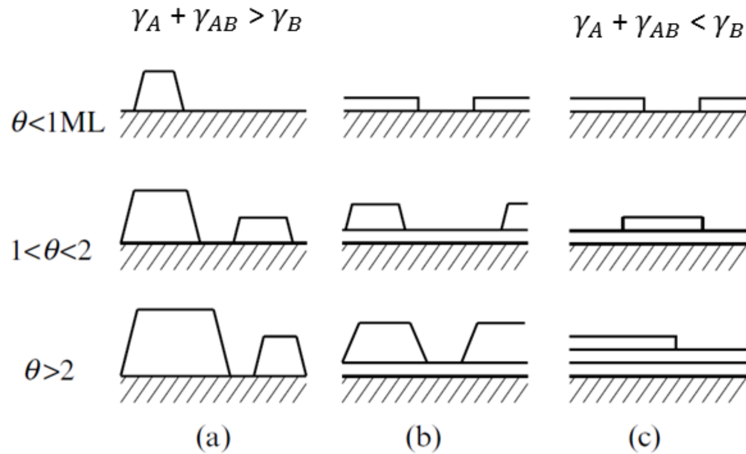

Figure I.6. Growth modes with surface energy considerations. γ_{AB} is the interfacial energy between the substrate B and the depositing film A. (a) represents Volmer-Weber or island growth, (b) Stranski-Krastanov or layer plus island, and (c) Frank-van der Merwe or layer by layer growth. (adapted from [22], p. 146).

For materials that are closely matched in energy like the Co/Cu system, these considerations are complicated. Co deposition on Cu may yield 2D films up to a finite thickness at which point the films roughen and grow three dimensionally. SK type growth might support that reconciliation of heteroepitaxial strain between the Co and Cu leads to the 2D-3D transition. Another explanation may be that the apparent transition from 2D to 3D growth reflects preferential deposition at grains of a specific crystallographic orientation [23–28]. That Co/Cu multilayers made for magnetic systems exhibit mixed hcp and fcc Co on fcc Cu (111) suggests that the latter theory is probable [26,27].

Area-selective ALD

Area-selective processes allow for the patterned deposition of one material onto another. Patterning may be achieved through processes like photolithography in which masks are used with light to selectively etch patterns into a light-sensitive photoresist film. It is also possible to match existing patterns, e.g., Cu lines in a BEOL metallization layer,

by leveraging chemical selectivity such that deposition only occurs in desired areas. Physical patterning like photolithography and self-assembled monolayers have many interesting applications and might be used to selectively deposit Co capping layers. However, these processes generally require many more preparation and post-processing steps making them less desirable than processes that rely only on chemical selectivity. As previously mentioned, CoWP capping layers for Cu interconnects may be selectively deposited by electroless deposition. Nevertheless, post-processing surface cleaning steps are necessary and, ultimately, the plating bath can contaminate the ILD [4,5]. Consequently, next generation deposition processes like selective ALD are of great interest to develop ultrathin metal caps.

For selective ALD to work, it is important to tune the precursor and substrate surface chemistries as well as the operating conditions. Specifically, the precursor should deposit preferentially on the desired surface or methods to chemically passify the adjacent surfaces should be used. Further, exceeding the ALD temperature window can lead to thermal degradation of the precursor leading to loss of selectivity. For BEOL materials the disparity between the Cu metal surface and the reactive surface species on the ILD materials lends itself to chemically-selective ALD.

BEOL Materials – Surface Chemistry Considerations

Silicon dioxide surface chemistry is well documented experimentally and theoretically [22-24]. According to the Zhuravlev model, SiO_2 surfaces after an HF etch and vacuum annealing to 250 °C are fully hydroxylated (~4.6 OH/nm^2) with no residual physisorbed water. Apart from OH surface species, SiO_2 surfaces comprise Si-O-Si bonds in the form of siloxane bridges. After neighboring OH moieties on SiO_2 are condensed under annealing, they form strained siloxane bridges that relax to stable Si-O-Si bonds if annealed > 400 °C. Strained siloxane bridges are generally less stable and more reactive

than relaxed siloxane bridges but less reactive than surface OH species [23]. Stable siloxane bridges do not generally hydrogen bond and are hydrophobic, whereas the shifted electron density in strained siloxanes allows for hydrogen bonding and more reactivity.

Due to the large concentration of Si-CH_3 terminations in CDO, it exhibits fewer of the same reactive surface sites than SiO_2. The concentration of reactive surface sites, especially OH moieties, holds important implications for the ALD and passivation strategies that facilitate selective ALD. To target surface OH for passivation, silane chemistries including amino-silanes and chlorosilanes are explored for their effectiveness at inhibiting Co nucleation on SiO_2 and CDO while leaving the accumulation on Cu unaffected.

It has been demonstrated that transition-metal amidinate precursor chemistries readily deposit on other transitional metal surfaces with H_2 or NH_3 coreactants [25–29]. In particular bis(N-tert-butyl-N'-ethylpropionamidinato) cobalt(II) CoAMD has shown promise as a CVD or ALD precursor for Co thin films deposition and will be the focus of this work [30,31].

I.4 Objectives and Overview of Chapters

The purpose of this work is to investigate chemical methods that improve metal nucleation and support the development of selective ALD of Co metal capping layers on BEOL Cu interconnects.

Chapter 1 examines the adsorption behavior of a chelating Co ALD precursor on Cu, SiO_2, and CDO. Adsorption of the atomic layer deposition (ALD) precursor bis(N-tert-butyl-N'-ethylpropionamidinato) cobalt(II) (CoAMD) on SiO_2, carbon-doped oxide (CDO), and Cu is reported. Adsorption was performed under ALD cycling conditions with and without H_2 coreactant to mimic the first and second ALD half reactions on the substrates. Resultant surface chemistries were evaluated by X-ray photoelectron

spectroscopy (XPS). Adsorption of CoAMD proved self-limiting and the precursor reduced readily on Cu with and without H_2 coreactant to form Co^0. Residual C and N signals on Cu suggest that amidinate ligands and decomposition fragments from CoAMD adsorb on the Cu surface. On SiO_2 and CDO, CoAMD chemisorbs on O containing moieties, primarily OH, to form Co^{2+}. Accumulation of Co after three ALD cycles was greatest on Cu and least on CDO.

Chapter 1.2 evaluates the Co film properties as deposited on Cu substrates. Co films were deposited on Cu substrates at 265 °C by ALD with H_2 coreactant from the chelating Co amidinate precursor bis(N-tert-butyl-N'-ethylpropionamidinato) cobalt(II) (CoAMD). The deposited films were depth profiled with *ex situ* time-of-flight secondary ion mass spectrometry (ToF-SIMS) to reveal film properties. XPS, atomic force microscopy (AFM), scanning and transmission electron microscopy (SEM and TEM, respectively) measurements reveal additional film characteristics. The data suggest Stranski-Krastanov deposition comprising a Co wetting layer, and, at the surface, Co islands resulting from reconciliation of the heteroepitaxial strain between the mismatched Co and the FCC Cu substrate. Moreover, XPS and ToF-SIMS data reveal that Cu diffuses through the Co film, likely at facile Cu diffusion pathways along the polycrystalline Co grain boundaries, and that some Cu segregates to the surface of the Co during deposition. The surface-segregated Cu is believed to stabilize Co nucleation and film growth against the Co/Cu lattice mismatch strain and minimize the free surface energy. Strong Co/Cu intermixing suggest a complex chemical interaction between CoAMD and Cu under ALD conditions.

Chapter 1.3 evaluates the chemical passivation of reactive surface sites on CDO to enable selective ALD of Co on Cu features in BEOL metallization structures. ALD of the precursor bis(*N*-tert-butyl-*N'*-ethylpropionamidinato) cobalt(II) (CoAMD) on relevant

BEOL materials, *e.g.*, SiO_2, CDO, and Cu has been demonstrated. CoAMD was evaluated for its inherent deposition selectivity on Cu versus CDO and SiO_2. Selectivity enhancing passivants were employed to inhibit the reactivity of the dielectric surfaces to CoAMD. CoAMD deposited preferentially on the Cu surface which interacts favorably with AMD type ligands. Accumulation of Co was appreciable on SiO_2 due to reactive free hydroxyl species and slowest on CDO which exhibited fewer reactive sites at which CoAMD could adsorb and nucleate. Trimethylchlorosilane (TMCS) most effectively eliminated CoAMD nucleation on SiO_2 and CDO without hindering Co accumulation on Cu substrates. Hexamethyldisilizane also reduced the surface reactivity of SiO_2 and CDO but required considerably higher exposures than TMCS to effect the same passivation and, ultimately, reduced Co accumulation on Cu as well.

Additional Research

A second section is presented of separate work performed during this Ph.D. study. Namely, Chapter 5 discusses the use of hot-wire filament cracked B_2H_6 (diborane) to create substitutional impurities in a graphite lattice to act as preferred nucleation and adhesion sites. The nucleation of Pt particles from $CH_3CpPt(CH_3)_3$ on boron-treated highly oriented pyrolytic graphite (HOPG) was investigated. HOPG was enhanced with B from diborane using hot wire chemical vapor deposition to generate BDx fragments that dissociatively adsorbed on the HOPG surface and subsequently reacted with the sp^2 C lattice. Unreacted BD_x fragments either reacted with the HOPG or desorbed during annealing. Pt was deposited using chemical vapor deposition. Platinized B-treated HOPG samples exhibited enhanced Pt dispersion and uniform nucleation as compared with cleaved and annealed HOPG samples. Pt particle density is shown to be tunable using varying B exposures. This study demonstrates that the optimization of Pt dispersion and adhesion to HOPG substrates is achievable using a scalable chemical enhancement method.

I.5 REFERENCES

[1] C. S. Hau-Riege, "An introduction to Cu electromigration," *Microelectron. Reliab.*, vol. 44, no. 2, pp. 195–205, Feb. 2004.

[2] M. Hauschildt, M. Gall, P. Justison, R. Hernandez, M. Herrick, S. Ogawa, P. S. Ho, and E. Zschech, "Large-Scale Statistical Study of Electromigration Early Failure for Cu/low-k Interconnects," *AIP Conf. Proc.*, vol. 945, pp. 66–81, 2007.

[3] "International Technology Roadmap for Semiconductors - Interconnect," 2011.

[4] A. Ceyhan and A. Naeemi, "Cu / Low- k Interconnect Technology Design and Benchmarking for Future Technology Nodes," *IEEE Trans. Electron Devices*, vol. 60, no. 12, pp. 4041–4047, 2013.

[5] K. M. Thom, "Growth and Characterization of Ru Films Deposited by Chemical Vapor Deposition : Towards Enhanced Nucleation and Film Properties," University of Texas at Austin, 2009.

[6] J. Shin, "Growth and Characterization of CVD Ru and Amorphous Ru-P Alloy Films for Liner Application in Cu Interconnect.," University of Texas at Austin, 2007.

[7] T. Yoda and H. Miyajima, "Advanced BEOL Technology Overview," in *Advanced Nanoscale ULSI Interconnects: Fundamentals and Applications*, 2009, pp. 275–298.

[8] C. S. Hau-Riege and C. V. Thompson, "Electromigration in Cu interconnects with very different grain structures," *Appl. Phys. Lett.*, vol. 78, no. 22, pp. 3451–3453, 2001.

[9] C.-K. Hu, L. Gignac, R. Rosenberg, E. Liniger, J. Rubino, C. Sambucetti, A. Domenicucci, X. Chen, and a. K. Stamper, "Reduced electromigration of Cu wires by surface coating," *Appl. Phys. Lett.*, vol. 81, no. 10, pp. 1782–1784, 2002.

[10] B. D. Hatton, K. Landskron, W. J. Hunks, M. R. Bennett, D. Shukaris, D. D. Perovic, and G. A, "Materials chemistry for low-k materials," *Mater. Today*, vol. 9, no. 3, pp. 22–31, 2006.

[11] C.-K. Hu, L. Gignac, S. G. Malhotra, R. Rosenberg, and S. Boettcher, "Mechanisms for very long electromigration lifetime in dual-damascene Cu interconnections," *Appl. Phys. Lett.*, vol. 78, no. 7, pp. 904–906, 2001.

[12] Z.-J. Wu, L. Cao, J. Im, K.-D. Lee, and P. S. Ho, "Critical initial void growth for electromigration: Stress modeling and multi-link statistics for Cu/low-k interconnects," *2013 IEEE Int. Interconnect Technol. Conf. - IITC*, pp. 1–3, Jun. 2013.

[13] T. Kirimura, K. Croes, Y. K. Siew, K. Vanstreels, P. Czarnecki, Z. El-mekki, M. H. Van Der Veen, D. Dictus, A. Yoon, A. Kolics, J. Bömmels, and Z. Tökei, "Void

nucleation and growth during electromigration in 30 nm wide Cu lines : Impact of different interfaces on failure mode,” *IEEE*, 2013.

[14] C.-C. Yang, P. Flaitz, P.-C. Wang, F. Chen, and D. Edelstein, “Characterization of Selectively Deposited Cobalt Capping Layers: Selectivity and Electromigration Resistance,” *IEEE Electron Device Lett.*, vol. 31, no. 7, pp. 728–730, Jul. 2010.

[15] R. G. Filippi, P.-C. Wang, a. Brendler, K. Chanda, and J. R. Lloyd, “Implications of a threshold failure time and void nucleation on electromigration of copper interconnects,” *J. Appl. Phys.*, vol. 107, no. 10, p. 103709, 2010.

[16] J. P. Gambino, “Improved Reliability of Copper Interconnects Using Alloying,” in *IPFA 2010: 17th IEEE International Symposium on the Physical and Failure Analysis of Integrated Circuits*, 2010.

[17] O. Aubel, C. Hennesthal, M. Hauschildt, A. Beyer, J. Poppe, G. Talut, M. Gall, J. Hahn, J. Boemmels, M. Nopper, and R. Seidel, “Backend-of-Line Reliability Improvement Options for 28nm Node Technologies and Beyond,” *IEEE*, pp. 26–28, 2011.

[18] O. Aubel, J. Hohage, F. Feustel, C. Hennesthal, U. Mayer, A. Preusse, M. Nopper, and M. U. Lehr, “Process options for improving electromigration performance in 32nm technology and beyond,” in *IEEE: 47th Annual International Reliability Physics Symposium*, 2009, pp. 832–836.

[19] L. B. Henderson and J. G. Ekerdt, “Chemically capping copper with cobalt,” *Microelectron. Eng.*, vol. 87, no. 4, pp. 588–592, Apr. 2010.

[20] O. Aubel, S. Thierbach, R. Seidel, B. Freudenberg, M. A. Meyer, F. Feustel, J. Poppe, M. Nopper, A. Preusse, and C. Zistl, “Comprehensive reliability analysis of CoWP Metal Cap unit processes for high volume production in sub-µm dimensions,” pp. 675–676, 2008.

[21] C. Chou and W. Dow, “Formation of CoWP Barrier Layer by Electroless Deposition for TSV Metallization,” p. 2010.

[22] J. A. Venables, *Introduction to Surface and Thin Film Processes*. New York, NY: Cambridge University Press, 2000.

[23] O. Nilsen, O. B. Karlsen, A. Kjekshus, and H. Fjellvåg, “Simulation of growth dynamics in atomic layer deposition. Part I. Amorphous films,” *Thin Solid Films*, vol. 515, no. 11, pp. 4527–4537, Apr. 2007.

[24] O. Nilsen, O. B. Karlsen, A. Kjekshus, and H. Fjellvåg, “Simulation of growth dynamics for nearly epitaxial films,” *J. Cryst. Growth*, vol. 308, no. 2, pp. 366–375, Oct. 2007.

[25] O. Nilsen, O. B. Karlsen, A. Kjekshus, and H. Fjellvåg, “Simulation of growth dynamics in atomic layer deposition. Part II. Polycrystalline films from cubic crystallites,” *Thin Solid Films*, vol. 515, no. 11, pp. 4538–4549, Apr. 2007.

[26] O. Nilsen, O. B. Karlsen, A. Kjekshus, and H. Fjellvåg, "Simulation of growth dynamics in atomic layer deposition. Part III. Polycrystalline films from tetragonal crystallites," *Thin Solid Films*, vol. 515, no. 11, pp. 4550–4558, Apr. 2007.

[27] B. P. Tonner, Z.-L. Han, and J. Zhang, "Structure of Co films grown on Cu(111) studied by photoelectron diffraction," *Phys. Rev. B*, vol. 47, no. 15, pp. 9723–9732, 1993.

[28] H. Shimizu, K. Sakoda, T. Momose, and Y. Shimogaki, "Atomic Layer Deposited Co(W) Film as a Single-Layered Barrier/Liner for Next-Generation Cu-Interconnects," *Jpn. J. Appl. Phys.*, vol. 51, p. 05EB02, May 2012.

[29] F. J. Lamelas, C. H. Lee, H. He, W. Vavra, and R. Clarke, "Coherent fcc stacking in epitaxial Co/Cu superlattices," *Phys. Rev. B*, vol. 40, no. 8, pp. 5837–5840, 1989.

[30] J. de la Figuera, J. E. Prieto, and R. Miranda, "Scanning-tunneling-microscopy study of the growth of cobalt on Cu(111)," *Phys. Rev. B*, vol. 47, no. 19, pp. 13043–13049, 1993.

[31] H. Li, D. B. Farmer, R. G. Gordon, Y. Lin, and J. Vlassak, "Vapor Deposition of Ruthenium from an Amidinate Precursor," *J. Electrochem. Soc.*, vol. 154, no. 12, pp. D642–D647, 2007.

[32] J. Wu, J. Li, C. Zhou, X. Lei, T. Gaffney, J. a. T. Norman, Z. Li, R. Gordon, and H. Cheng, "Computational Study on the Relative Reactivities of Cobalt and Nickel Amidinates via β-H Migration," *Organometallics*, vol. 26, no. 11, pp. 2803–2805, May 2007.

[33] Z. Li, S. T. Barry, and R. G. Gordon, "Synthesis and characterization of copper(I) amidinates as precursors for atomic layer deposition (ALD) of copper metal.," *Inorg. Chem.*, vol. 44, no. 6, pp. 1728–35, Mar. 2005.

[34] H.-B.-R. Lee, W.-H. Kim, J. W. Lee, J.-M. Kim, K. Heo, I. C. Hwang, Y. Park, S. Hong, and H. Kim, "High Quality Area-Selective Atomic Layer Deposition Co Using Ammonia Gas as a Reactant," *J. Electrochem. Soc.*, vol. 157, no. 1, p. D10, 2010.

[35] R. G. Gordon, H. Kim, and H. Bhandari, "Cobalt Nitride Layers for Copper Interconnects and Methods for Forming Them," US 2008/0254232 A12008.

[36] H. B. Bhandari, J. Yang, H. Kim, Y. Lin, R. G. Gordon, Q. M. Wang, J.-S. M. Lehn, H. Li, and D. Shenai, "Chemical Vapor Deposition of Cobalt Nitride and its Application as an Adhesion-Enhancing Layer for Advanced Copper Interconnects," *ECS J. Solid State Sci. Technol.*, vol. 1, no. 5, pp. N79–N84, Sep. 2012.

[37] Z. Li, D. K. Lee, M. Coulter, L. N. J. Rodriguez, and R. G. Gordon, "Synthesis and characterization of volatile liquid cobalt amidinates.," *Dalton Trans.*, no. 19, pp. 2592–2597, May 2008.

SECTION 1: CHEMICAL SELECTIVITY IN ATOMIC LAYER DEPOSITION OF COBALT CAPPING LAYERS

Chapter 1: XPS investigation of the atomic layer deposition half reactions of bis(N-tert-butyl-N'-ethylpropionamidinato) cobalt(II)

1.1 INTRODUCTION

Economic and performance demands drive the scaling of microelectronics. Maintaining chip performance while reducing feature size involves many manufacturing and materials challenges. In particular, increasing current density in back end of line (BEOL) interconnects has led to premature chip failure from electromigration-induced Cu diffusion. Material interfaces, such as the Cu-interlayer dielectric (ILD) barrier interface, have been demonstrated as accelerated pathways for Cu electromigration (EM) [1-4]. Consequently, Cu EM challenges are an important focus of BEOL materials research [3,5-9]. To improve device lifetimes, EM can be reduced by alloying of Cu interconnects but depositing thin EM resistant metal caps on the metallization lines is preferred due to large resistivity increases associated with alloying [10,11]. As device scaling continues to the 7 nm node and beyond, capping layers will likely be necessary to mitigate Cu EM. Co makes an effective capping material and is less expensive than alternatives like Ru [10,11].

To ensure device performance and maintain a low RC constant, Co capping layers must resist Cu EM, deposit conformally, and be the thinnest possible continuous film [12]. Ideally, capping layers should also deposit selectively on Cu. Co has been demonstrated to deposit conformally on Cu using a variety of methods including chemical vapor or atomic layer deposition (CVD or ALD), physical vapor deposition (PVD), and electroless deposition [2,3,13]. Moreover, selective CVD of Co on Cu from a carbonyl-based precursor has been previously demonstrated [13]. Selective ALD processes are desirable

because they provide controlled deposition of film thicknesses below five nm and may be able to meet ITRS expectations of 0.5 nm barrier films by 2025 [14]. Enabling selective deposition avoids costly post processing inherent in lithography and physical deposition methods. To develop selective ALD of Co as a Cu EM barrier, this work investigates the relevant ALD half reactions of a chelated Co amidinate ALD precursor by focusing on the first few adsorption reaction cycles on Cu, SiO_2, and carbon-doped oxide (CDO) surfaces.

Chelated metal-organic precursors find widespread application in ALD processes [12,15-20]. Chelated amidinates in particular have become commonplace in metals deposition and a number are commercially available. For instance, Cu and Co amidinate (AMD) chemistries have shown promise for ALD and CVD using reducing coreactants H_2 and NH_3. Deposition of Co films from AMD complexes has been shown to be sensitive to temperature and coreactant species. Bis(*N,N'*-diisopropylacetamidinato)cobalt(II) is reported for ALD of thin Co films at substrate temperatures exceeding 260 °C with appreciable deposition rates beginning at 300 °C [12,17-19,21]. This study concerns itself with the less-reported bis(*N*-tert-butyl-*N'*-ethylpropionamidinato) cobalt(II), referred to herein as CoAMD. CoAMD is a liquid at room temperature with adequate vapor pressure at moderate temperature for inert sweep-based delivery. We demonstrate that CoAMD deposits readily on Cu surfaces at lower temperatures than bis(*N,N'*-diisopropylacetamidinato)cobalt(II), as low as 215 °C, potentially making it a better candidate for low-temperature ALD operations that are important in BEOL processing for which the thermal budget is of ongoing concern.

Silicon dioxide surface chemistry is well documented experimentally and theoretically [22-24]. According to the Zhuravlev model, SiO_2 surfaces after HF etch and vacuum annealing to 250 °C are fully hydroxylated (~4.6 OH/nm^2) with no residual physisorbed water. Apart from OH surface species, SiO_2 surfaces comprise Si-O-Si bonds

in the form of siloxane bridges. After neighboring OH moieties on SiO_2 are condensed under annealing, they form strained siloxane bridges that relax to stable Si-O-Si bonds if annealed > 400 °C. Strained siloxane bridges are generally less stable and more reactive than relaxed siloxane bridges but less reactive than surface OH species [23]. Stable siloxane bridges do not generally hydrogen bond and are hydrophobic, whereas the shifted electron density in strained siloxanes allows for hydrogen bonding and more reactivity.

CDO substrates with dielectric constants between 2 and 3 are generally highly methlylated amorphous SiO_2, leading to a large concentration of Si-CH_3 terminations, and are semi-porous. Consequently, CDO exhibits fewer of the same reactive surface sites than SiO_2. In fact, freshly cleaned SiO_2 is fully wetted by water, whereas cleaned CDO is hydrophobic, yielding water contact angles in excess of 60° with no additional treatment (Goniometer measurements not shown). The concentration of reactive surface sites, especially OH moieties, holds important implications for the expected ALD half-reactions of the first monolayers and of the incubation period for ALD deposition, which depends on the chemical nature of the adsorption site(s) and their reactivity. It is expected that CDO, with a lower surface OH concentration, will accumulate Co less quickly than fully hydroxylated SiO_2.

1.2 Experimental Section

SiO_2 (600 nm thermal oxide), CDO (k ~ 2.6), and Cu (300 nm PVD on Si) substrates were provided by Intel. AccuDep® CoAMD was supplied by Dow Chemical and used without modification. Coreactant H_2 and Ar sweep gases were provided by Matheson (99.999%). The as-received substrates were cleaned by rinsing, in order, with acetone, ethanol (Fisher ACS grade), and deionized (DI) water (18.2 MΩ cm). Following the rinse, Cu substrates were cleaned of the majority of the surface oxide by etching in 35 °C glacial acetic acid (99.9%, Fisher Scientific) for 1 min [25]. SiO_2 samples were placed

in a piranha bath (6 : 2 : 1 - H_2SO_4 (Fisher ACS plus) : H_2O_2 (Fisher 30%) : DI H_2O) for 15 min followed by a 10 s HF (2% in H_2O) etch. CDO was cleaned in a 1 : 1 : 1 tetramethylammoniumhydroxide (Acros Organics 25% in H_2O) : ethylene glycol (Fisher) : DI H_2O bath for 2 min at 50 °C.

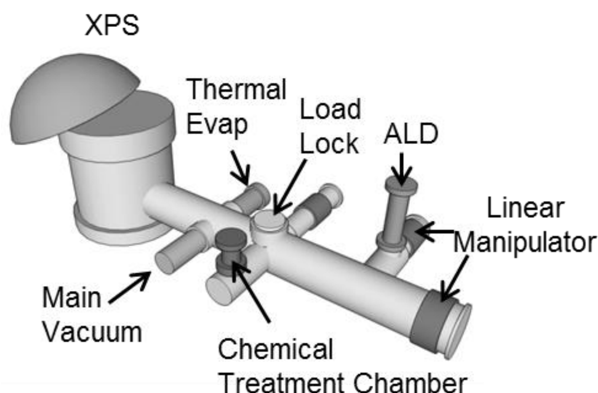

Figure 1.1. ALD and analysis chamber.

Cleaned samples were transferred via load lock into a previously described, in-house built ALD system (Figure 1.1) [26]. The ALD system comprises *in situ* transfer between a hot-walled ALD chamber and an analysis chamber. The analysis chamber houses an X-ray photoelectron spectrometer (PHI model 1600/2057) with Ar^+ sputtering capabilities.

Adsorption experiments were performed in the ALD chamber. Within the ALD chamber, substrates are positioned perpendicular to the flow of precursors and reactant gases. The CoAMD is held at 80 °C and delivered by 50 sccm Ar carrier gas. An upstream, heated diffusion plate is employed to improve mixing during ALD to facilitate even substrate surface exposure to the process gases. Calibrated substrate surface temperatures are measured relative to a K-type thermocouple positioned just below the substrate. Substrate surface temperatures were 265 °C for ALD cycling unless otherwise specified.

The ALD base operating pressure is 260 mTorr and is a function of the gas flow and pumping rates. During adsorption experiments, the respective substrates were exposed to ALD cycling of CoAMD, Ar purge and carrier gas, and H_2 coreactant. The exposures were controlled by temperature, mass flow, and time of exposure via automated pneumatic valves. A typical ALD cycle comprises a 2 s CoAMD exposure, corresponding to ~7×10^5 L including Ar carrier gas fed at 50 sccm (1L = 1×10^{-6} torr×s), and 15 s H_2 coreactant exposures (1.0×10^7 L) separated by 15 s Ar purges (5.4×10^6 L). Three different ALD schemes were employed: one cycle without H_2 (1×2s no H_2), one cycle with H_2 (1×2s), and 3 cycles with H_2 (3×2s). Exposures were varied between one and three ALD cycles to demonstrate Co accumulation and the influence of the H_2 coreactant on the reduction and dissociation of adsorbed AMD ligands from the respective substrates. Condensation experiments comprised one 4 s CoAMD exposure (1.4×10^5 L) without H_2 at a substrate temperature of 100 °C.

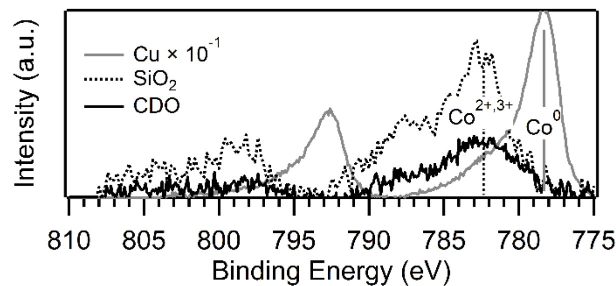

Figure 1.2. Co 2*p* XP spectra of 3x2s CoAMD cycles on the respective substrates. All signals have been normalized with background subtraction (Shirley type). The Co signal intensity on Cu is reduced by one order of magnitude.

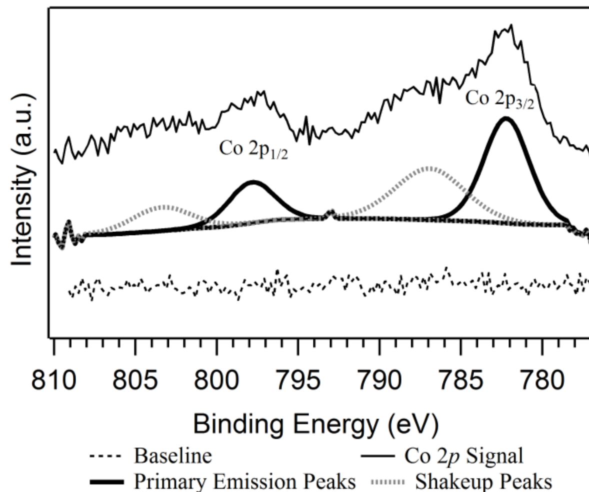

Figure 1.3. Co 2*p* XP spectrum following a 1×4s-no-H_2 CoAMD exposure on SiO_2 at 100 °C.

1.3 Results

CoAMD was adsorbed under ALD cycling conditions on SiO_2, CDO, and Cu substrates and the resulting surface species were analyzed by X-ray photoelectron spectroscopy (XPS). One CoAMD ALD cycle, with and without H_2 coreactant, and three ALD cycle adsorptions with H_2 were performed to understand the relative reactivity of the precursor on the three substrates and the surface reactions that lead to Co nucleation.

Figure 1.2 depicts Co XP spectra of 3×2s CoAMD cycle adsorptions on each of the substrates. The figure indicates the difference in Co oxidation state on the respective substrates. Co is mostly reduced on Cu with a Co 2p3/2 binding energy (BE) of 778.3 eV. The Co $2p_{3/2}$ BE for CoAMD adsorbed on SiO_2 and CDO at 782.5 eV is consistent with Co^{2+} and Co^{3+}; Co $2p_{3/2}$ and Co $2p_{1/2}$ shakeup peaks at 788 and 804V, respectively, on SiO_2 and CDO correspond to paramagnetic Co^{2+} indicating the Co is in an oxidized state on these substrates. In separate experiments, SiO_2 and CDO were exposed to CoAMD at 100 °C for 1×4s-no-H_2 exposure. Figure 1.3 presents the resulting Co 2*p* spectrum from the

SiO_2 substrate. The figure serves to better illustrate the Co 2*p* primary emission and shakeup peaks corresponding to Co^{2+}.

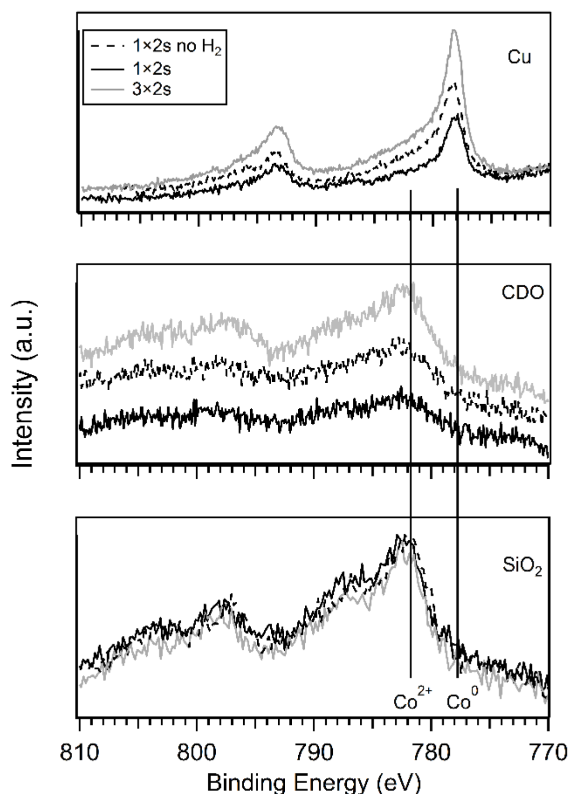

Figure 1.4. Co 2*p* XP spectra from adsorption cycling on each substrate. The spectra indicate oxidized Co formed on SiO_2 and CDO and reduced Co formed on Cu, with or without H_2 exposure.

Figure 1.4 demonstrates Co accumulation on each substrate after 1 or 3 ALD cycles. The Co XP spectra show step-wise accumulation on Cu and CDO upon increasing the total exposure. The amount of Co accumulated on SiO2 did not increase from 1 – 3 cycles. A comparison of the 1×2s with 1×2s-no-H_2 spectra illustrate that CoAMD adsorbs and transforms into Co0 on Cu before the addition of H_2 and is unchanged after one complete ALD cycle, i.e., after 1×2s.

After 1×4s-no-H_2 exposure at 100 °C, 2.53 at. % Co was observed on SiO_2 (Figure 1.3) while 2.52 at. % adsorbed on CDO (not shown). Further, 1.28 at. % and 2.01 at. % N was observed on SiO_2 and CDO, respectively. The Co:N atomic ratio for CoAMD is 0.25 : 1. After 1×4s-no-H_2 at 100 °C and 3×2s at 265 °C on SiO2, the Co:N ratios were 1.98 : 1 and 5.09 : 1, respectively. On CDO, the corresponding Co:N ratios were 1.25 : 1 and 1.15 : 1, respectively.

The adsorption of CoAMD on Cu is self-limiting and the saturation exposure of CoAMD was determined on the Cu substrate by 1× ALD exposures at 265 °C. By XPS, the Co:Cu ratio is 0.19 : 1 after 1×2s exposure, 0.38 : 1 after 1×4s, and 0.35 : 1 after 1×10s exposure. Therefore, 1× exposures saturate the Cu surface by 4 s after which Co does not continue to accumulate without a coreactant cycle. It was also observed that the addition of H_2 causes a slight reduction in Co signal intensity relative to a 1×2s-no-H_2 exposure (Figure 1.4).

The effect of temperature on Co accumulation on Cu was studied from 215-290 °C (Figure 1.5). The greatest accumulation after 3 ALD cycles occurs at 265 °C; however, the accumulation at 215 °C is not substantially reduced in magnitude. Therefore, the ALD process with CoAMD affords a larger temperature range than has been used with the bis(N,N'-diisopropylacetamidinato) cobalt(II) precursor and may be relevant for low or reduced temperature ALD applications [12,17-19,21].

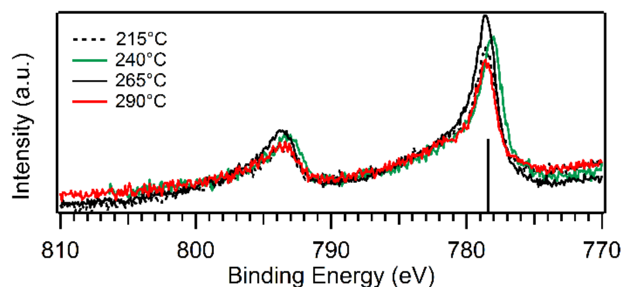

Figure 1.5. 3×2s CoAMD adsorption on Cu at different temperatues. Co 2$p_{3/2}$ signals indicate reduced Co^0 (778.3eV) for all tested substrate temperatures.

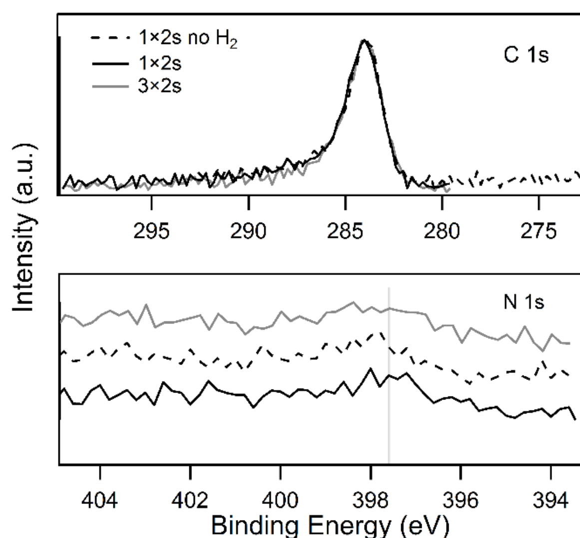

Figure 1.6. Residual C 1*s* and N 1*s* spectra on Cu after 1 or 3 ALD cycles and after one CoAMD half-cycle. N is present in small amounts. N 1*s* signals overlap but are offset deliberately for clarity.

Residual C and N signals on Cu (Figure 1.6) following 1 or 3 ALD cycles and after the first CoAMD half-cycle at 265 °C demonstrate that CoAMD may readily give up its ligands to the Cu surface and the subsequent desorption of those ligands is incomplete. While the majority of the AMD fragments are removed during the inert gas sweep and the second half-cycle, some AMD fragments are incorporated into the subsequent Co film as

C and N impurities. 800 ALD cycles on Cu at 265 °C (not shown) indicate that 4.4 nm thick Co films contain about 17 at. % C and 2 at. % N.

1.4 DISCUSSION

The scheme in Figure 1.7 suggests a possible ALD process for CoAMD on the Cu surface. The affinity of AMD fragments for transition metal surfaces leads to the initial dissociative chemisorption of CoAMD on Cu during which the AMD fragments complex with the Cu surface. Ma, et al. previously demonstrated that adsorbed AMD ligands undergo complex decomposition and desorption mechanisms on transition metals [27]. In particular, it is likely that the CoAMD fragments partially decompose on the Cu surface leaving residual amidinate and alkyl fragments. AMD ligand and fragment desorption is likely incomplete before the next ALD cycle for reasonable purge times. Incomplete ligand desorption leads to C and N incorporation as film impurities (Figure 1.6).

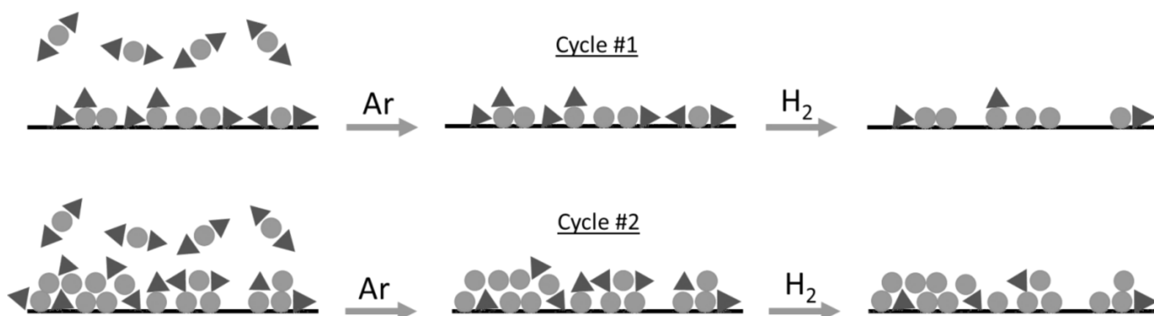

Figure 1.7. One possible dissociative adsorption process of CoAMD on Cu during ALD cycling is depicted (the Ar purge after the H_2 exposure in the second half reaction is not shown). Circles represent Co and triangles represent amidinate ligands and fragments from the CoAMD precursor while the black line represents the Cu surface.

The ALD of Co on Cu from CoAMD appears limited by the reaction and desorption of the AMD ligand fragments, which requires exposure to a coreactant like H_2 or NH_3. H_2 exposure decreased the Co signal intensity on Cu relative to 1×2s-no-H_2 exposure (Figure

1.4) suggesting that CoAMD may form a partial multilayer that is not fully removed during the Ar purge step. Close inspection of the high BE shoulder of the 1×2s Co $2p_{3/2}$ peak indicates some higher oxidation state of Co is present on Cu before H_2 exposure. In order to mitigate multilayer formation and better reflect the interaction between CoAMD and the Cu substrate, 2 s rather than 4 s CoAMD cycles comprise the majority of our experiments.

The presence of Co^{2+} (Figure 1.2) and the Co:N ratios greater than 0.25 : 1 on CDO and SiO_2 indicates that CoAMD dissociatively chemisorbs at O containing surface moieties on CDO and SiO_2. In particular, reactive surface (OH) species are suspected as the primary sites for Co nucleation on SiO_2. Dai, et al. demonstrated that the Cu amidinate, copper(I) di-sec-butylacetamidinate, reacts at (OH) ligands on SiO_2 surfaces to form Si-O-CuR linkages [28]. We expect CoAMD behaves similarly on hydroxylated SiO_2 and CDO surfaces resulting in Si-O-CoR linkages. On CDO, many Si atoms are methylated. Therefore, O-based surface species are expected in lower concentrations than on SiO_2, resulting in fewer facile Co nucleation sites and slower Co accumulation on CDO relative to SiO_2. This is supported by the greater accumulation of Co on SiO_2 versus CDO after one cycle at which point facile nucleation sites on SiO_2 are saturated (Figure 1.4). After three cycles, the Co concentration on CDO and SiO_2 is, 1.7 at. % and 2.5 at. %, respectively.

On CDO, the smaller Co:N ratio after 1×4s-no-H_2 exposure at 100 °C indicates more unreacted or partially reacted CoAMD on its surface than on SiO_2. Further, the fact that Co:N is high on CDO and SiO_2, 8 times and 5 times what is present in unreacted CoAMD, suggests that most adsorbed CoAMD on both surfaces have lost one AMD ligand and many have fully reacted at the surface. Though the broadness of the primary emission peak could indicate some Co^{3+} character, the shakeup peaks indicate paramagnetic Co^{2+}. Additionally, the ratio of the shakeup peaks to the primary peaks is effectively unchanged between the 1×4s no H_2 exposure at 100 °C and 3×2s exposure at 265 °C indicating that

the average Co oxidation state is unchanged from Co^{2+} on the dielectric surfaces. Although dissociation was unexpected at this temperature, Ma *et al.* have recently reported that copper(I)-N,N'-di-sec-butylacetamidinate partially dissociated at temperatures as low as -73 °C on Ni(110) [27]. The apparent partial dissociation of CoAMD on SiO_2 and CDO at 100 °C speaks to the reactivity of CoAMD and to the reactivity of the available surface O and, especially, OH groups. After 3×2s adsorption on SiO_2, the Co:N ratio is 20 times that of CoAMD and indicates that H_2 coreactant cycles readily clear N moieties from the surface. On the other hand, the Co:C ratio after 3×2s adsorption on SiO_2 is only 6 times that expected from CoAMD, suggesting that C moieties bond more strongly to the surface. Ma *et al.*'s Cu amidinate work indicates that C does not fully desorb from Ni surfaces even as substrates are annealed up to 800 K [27]. The net accumulation of Co on SiO_2 after 1×4s no H_2 exposures at 100 °C and 3×2s exposures at 265 °C was 2.53 and 2.7 at. %, respectively, suggesting that multilayer adsorption occurs especially at low temperatures. Further, while the Co accumulation after 1×4s no H_2 exposures on CDO and SiO_2 was the same, the accumulation on CDO was 30% lower than on SiO_2 after 3×2s cycling. This indicates both multilayer adsorption on the CDO and that the SiO_2 surface comprises more reactive surface sites than CDO.

The difference in Co accumulation on the respective surfaces is an indication of the nature of CoAMD chemisorption on each substrate. On a metal surface, the precursor and dissociated AMD ligands compete for metal adsorption sites. Whereas, Co accumulation on SiO_2 saturates after the first cycle indicating that the most reactive surface sites, OH groups, are populated very quickly under ALD conditions. After the OH sites are occupied, CoAMD must react at previously adsorbed Co or less-reactive siloxane bridges. Due to its lower OH surface concentration, CDO exhibits slower initial Co accumulateion than SiO_2.

Extended Co depositions, reported elsewhere, confirm that Co continues to nucleate at Co islands and O surface species.

1.5 CONCLUSIONS

The interactions of CoAMD on Cu, SiO_2 and CDO were investigated by XPS. Co from CoAMD accumulates preferentially on Cu metal substrates via a complex dissociative chemisorption mechanism. Accumulation of Co on Cu from CoAMD is ALD-like and self-limiting; the desorption of chemisorbed AMD ligand fragments is completed during exposure to a reducing coreactant like H_2. CoAMD interactions with SiO_2 and CDO surfaces appear strongest with exposed OH moieties as indicated by faster initial accumulation of CoAMD on SiO_2 than on CDO but may also deposit on strained siloxane surface species. CoAMD readily deposits at existing, unoccupied Co surface species. Both SiO_2 and CDO favored the formation of oxidized Co species and some partially reacted CoAMD precursor. The inherent preference of CoAMD to deposit on transition metals like Cu versus dielectric surfaces bodes well for applications in selective ALD.

1.6 REFERENCES

[1] Hu, C.-K.; Gignac, L.; Malhotra, S. G.; Rosenberg, R.; Boettcher, S. Appl. Phys. Lett. 2001, 78, 904–906.y

[2] Hu, C.-K.; Gignac, L.; Rosenberg, R.; Liniger, E.; Rubino, J.; Sambucetti, C.; Domenicucci, a.; Chen, X.; Stamper, a. K. Appl. Phys. Lett. 2002, 81, 1782-1784.

[3] Hau-Riege, C. S. Microelectron. Reliab. 2004, 44, 195–205.

[4] Ding, P. J.; Lanford, W. A.; Hymes, S.; Murarka, S. P. Appl. Phys. Lett. 1994, 64, 2897–2899.

[5] Wu, W.; Yuan, J. S. Solid. State. Electron. 2011, 45, 2011–2016.

[6] Kaanta, C. W.; Bombardier, S. G.; Cote, W. J.; Hill, W. R.; Kerszykowski, G.; Landis, H. S.; Poindexter, D. J.; Pollard, C. W.; Ross, G. H.; Ryan, J. G.; Wolff, S.; Cronin, J. E. 1991 Proc. Eighth Int. IEEE VLSI Multilevel Interconnect. Conf. 1991, 144–152.

[7] Hau-Riege, C. S.; Thompson, C. V. Appl. Phys. Lett. 2001, 78, 3451–3453.

[8] Arnaud, L.; Cacho, F.; Doyen, L.; Terrier, F.; Galpin, D.; Monget, C. Microelectron. Eng. 2010, 87, 355–360.

[9] Arnaud, L.; Tartavel, G.; Berger, T.; Mariolle, D.; Gobil, Y.; Touet, I. In 37th Annual International Reliability Physics Symposium; San Diego, CA, 1999; pp. 263–269.

[10] Gambino, J. P. In IPFA 2010: 17th IEEE International Symposium on the Physical and Failure Analysis of Integrated Circuits; IEEE, 2010.

[11] Aubel, O.; Hennesthal, C.; Hauschildt, M.; Beyer, A.; Poppe, J.; Talut, G.; Gall, M.; Hahn, J.; Boemmels, J.; Nopper, M.; Seidel, R. IEEE 2011, 26–28.

[12] Lim, B. S.; Rahtu, A.; Gordon, R. G. Nat. Mater. 2003, 2, 749–754.

[13] Yang, C.-C.; Flaitz, P.; Wang, P.-C.; Chen, F.; Edelstein, D. IEEE Electron Device Lett. 2010, 31, 728–730.

[14] Iwai, H. Microelectron. Eng. 2009, 86, 1520–1528.

[15] Li, H.; Farmer, D. B.; Gordon, R. G.; Lin, Y.; Vlassak, J. J. Electrochem. Soc. 2007, 154, D642- D647.

[16] Li, Z.; Barry, S. T.; Gordon, R. G. Inorg. Chem. 2005, 44, 1728–35.

[17] Li, Z.; Lee, D. K.; Coulter, M.; Rodriguez, L. N. J.; Gordon, R. G. Dalton Trans. 2008, 2592–2597.

[18] Lim, B. S.; Rahtu, A.; Park, J.-S.; Gordon, R. G. Inorg. Chem. 2003, 42, 7951–7958.

[19] Lee, H.-B.-R.; Kim, W.-H.; Lee, J. W.; Kim, J.-M.; Heo, K.; Hwang, I. C.; Park, Y.; Hong, S.; Kim, H. J. Electrochem. Soc. 2010, 157, D10-D15.

[20] Bahlawane, N.; Kohse-Höinghaus, K.; Premkumar, P. A.; Lenoble, D. Chem. Sci. 2012, 3, 929–941.

[21] Gordon, R. G.; Kim, H.; Bhandari, H. Cobalt Nitride Layers for Copper Interconnects and Methods for Forming Them. U.S. Patent 0254232 A1, 2008.

[22] Kuo, C.-L.; Lee, S.; Hwang, G. Phys. Rev. Lett. 2008, 100, 1–4.

[23] Zhuravlev, L. T. Colloids Surfaces A Physicochem. Eng. Asp. 2000, 173, 1–38.

[24] McCrate, J. M.; Ekerdt, J. G. Langmuir 2013, 29, 11868–11875.

[25] Chavez, K. L.; Hess, D. W. J. Electrochem. Soc. 2001, 148, G640-G643.

[26] Wang, T.; Ekerdt, J. G. Chem. Mater. 2009, 21, 3096–3101.

[27] Ma, Q.; Guo, H.; Gordon, R. G.; Zaera, F. Chem. Mater. 2011, 23, 3325–3334.

[28] Dai, M.; Kwon, J.; Halls, M. D.; Gordon, R. G.; Chabal, Y. J. Langmuir 2010, 26, 3911–39177.

Chapter 2: Interdiffusion and diffusive stabilization of cobalt by copper during atomic layer deposition from bis(N-tert-butyl-N'-ethylpropionamidinato) cobalt(II)

2.1 INTRODUCTION

Known generally to exhibit good adhesion on Cu surfaces, Co and Co alloy films have recently been applied as Cu capping layers to mitigate premature microelectronic device failure due to Cu interconnect electromigration (EM) [1–3]. Decreasing microelectronic device dimensions continue to exacerbate the EM induced self-diffusion of Cu. Therefore, reducing Cu EM-induced failures in back end of line (BEOL) interconnects without increasing resistance-capacitive (RC) delay is an ongoing concern [4]. Cu alloys and EM-resistant metal capping layers are possible solutions to the EM challenge; however, capping is preferred to alloying due to resistivity increases associated with alloying Cu interconnects [5]. Co/Cu layers have been of great interest for many years for their applications in magnetic and microelectronic materials. The Co/Cu interface and structure has garnered particular interest and efforts have demonstrated lattice matching of Co on Cu (111) surfaces [6,7]. Further, Co capping layers have been demonstrated to reduce Cu EM more effectively than silicidation of the Cu surface. Co caps result in less resistance-capacitance increase in the metallization structure than SiCN caps and adhere better to Cu [1–3,5,8]. Currently selective, electrolessly deposited CoWP is a benchmark Cu EM barrier [1,3,5]. Nevertheless, contamination of the adjacent dielectric materials from the plating bath is a concern and much interest exists to develop alternative deposition methods [9]. Chemical vapor deposition (CVD) and atomic layer deposition (ALD) processes are of particular interest due to their ability to deposit ultrathin and conformal films and their potential application for surface selective deposition of barriers [10,11].

Previous work from Lim *et al.* demonstrated the deposition of Cu, Ni, and Co transition metals from a series of chelating amidinate precursors under ALD and CVD

conditions [12]. Bis(N-tert-butyl-N'-ethylpropionamidinato) cobalt(II) (CoAMD) is a proven ALD precursor for Co deposition that is amenable to carrier-gas-based vapor delivery and can be deposited using reducing agents like H_2 or NH_3 rather than O_2 [13]. Avoiding oxidation is important for BEOL components, especially the Cu metallization lines. We have separately demonstrated that CoAMD exhibits self-limiting adsorption on Cu and a preference to deposit on Cu rather than on SiO_2 or carbon-doped oxides that might comprise the BEOL interlayer dielectric materials [14]. The inherent selectivity of CoAMD for Cu over Si-based dielectric materials makes it an interesting candidate for selective-ALD processes.

In this study, we deposit sub-20 nm Co films by ALD from CoAMD on Cu to better understand the Co/Cu interface and Co film properties. Understanding the properties of ultrathin films is important for meeting the ITRS roadmap goal of 0.5 nm barrier films by 2025 [5]. *In situ* X-ray photoelectron spectroscopy (XPS) and *ex situ* depth profiling time of flight secondary ion mass spectrometry (ToF-SIMS) measurements reveal film composition. *Ex situ* characterization by scanning electron microscopy (SEM), cross-sectional transmission electron microscopy (TEM), and atomic force microscopy (AFM) provide structure and surface morphology of the films.

2.2 Experimental Section

AccuDep CoAMD was acquired from DOW and Cu substrates (300 nm PVD on Si) were provided by Intel. Co films were deposited by ALD in an in-house constructed vacuum system with *in situ* XPS. The vacuum system comprises a load lock and an ALD chamber with a base pressure of ~ 1×10^{-7} Torr and *in situ* transfer to a PHI model 1600 XPS for chemical analysis (base pressure ~1×10^{-9} Torr). System gases include Ar and H_2 (99.999 %, Matheson) each used with 50 sccm flow rate. Ar is used as the precursor carrier

gas and inert sweep. Prior to deposition, the Cu substrates were cleaned by rinsing in order with acetone, ethanol, and deionized water (18 MΩ) and then rinsed in a 35 °C bath of glacial acetic acid (99.9%, Fisher Scientific) for one min to remove surface oxide. The wafers were blown dry with pressurized Ar and loaded immediately into the vacuum system load lock. A typical ALD cycle comprises a 2-s CoAMD exposure and 15-s H_2 exposure separated by 15-s purges with Ar. Films are deposited at 265 °C with a precursor temperature of 80 °C.

Time of flight secondary ion mass spectrometry (ToF-SIMS) was employed to identify and spatially locate the species of interest throughout the films. Known as a highly elemental- and surface-sensitive analytical technique, ToF-SIMS comprises directing a high-energy but very low-intensity primary-ion beam onto a sample surface and analyzing the resulting ionized, ejected material (secondary ions, SI) by a time-of-flight technique. A TOF.SIMS 5 instrument (ION-TOF GmbH, 2010) was used for data acquisition. For depth-profiling chemical analysis of the Co films and Co/Cu interfaces, a short-pulsed (18 ns) primary ion beam (Bi_1^+, 30 keV energy, ~3.1 pA measured sample current) was typically raster-scanned over a 100×100 μm^2 area centered within a 250×250 μm^2 regressing area that was previously sputtered by a secondary-ion beam (Cs^+, 500 eV energy, ~53 nA measured sample current). The depth profiles were acquired at a base pressure of about 7.5×10^{-10} Torr in non-interlaced mode (i.e., sequential data acquisition and sputtering) and with the primary-ion beam set in high current bunched mode. All detected SI had negative polarity. The sputtering rates for Co and Cu were calculated as 1.2 Å/s and 2 Å/s, respectively, based on the TEM determined thicknesses and the corresponding time to sputter through the respective film layers. For converting the sputtering time, t, into a depth, z, a rate model assuming the instantaneous sputtering rate, $R(t)$, at the interface of

two films (referred to herein as A and B) as a linear combination of the individual sputtering rates was used [15]:

$$R(t) = \left|\frac{I(t)-I_B}{I_A-I_B}\right| R_A + \left|\frac{I(t)-I_A}{I_A-I_B}\right| R_B = \dot{z} \quad (1)$$

where $I(t)$ is the normalized secondary ion yield of a marker representative to one of the two films forming the interface, I_A and I_B are the values of $I(t)$ in the film A and B, respectively and R_A and R_B are the individual sputtering rates of the films A and B, respectively. The linear coefficients are essentially proportional to the molar fractions of the two materials at the sputtering time, t [16]. Following naturally, the sputtering depth, $z(t)$ corresponding to a certain sputtering time, t, reads:

$$z(t) = \int_{t_0}^{t} dt' R(t') \quad (2)$$

where t_0 is the initial sputtering time. Application of this model on the Cu_2 marker for Co/Cu interfaces leads to the conversion $t \rightarrow z(t)$. The Co_2 and Cu_2 secondary ions were chosen as markers for the Co and Cu films, respectively, to avoid the intrinsic artifacts Co and Cu signals have due to residuals originating from CoO and CuO, respectively.

To measure the atomic mixing between the Cu substrate and the Co overlayer the so called mixing-roughness-information (MRI) model was used [17]. This model states that (i) the real interface is a convolution between the interface roughness (roughness) and atomic mixing due to preparation and (ii) the measured interface in a depth profile is a convolution between the real interface, atomic mixing and roughness induced by sputtering, and information depth (i.e., depth of origin for the secondary ions). All these factors are represented by functions of depth whose lengths are essentially defined by their full width at half maximum (FWHM). The measured interface length is simply the sum in quadrature of all the factors that are convoluted. The atomic mixing due to sputtering and

the information depth are usually in the range of a few atomic layers and thus negligible with respect to the actual atomic mixing length. This is provided by the low energy (Cs^+, 500 eV) of the sputtering ion beam and the very low sputtering current of the probing beam (Bi_1^+, ~3 pA). Further, as the main interest is in the atomic mixing at the interface, the sputtering-induced interfacial roughness can be added to the intrinsic interfacial roughness originating from sample preparation. For inorganic (metallic) samples it was shown that the total roughness at the interface is an average of the roughness of the two individual films (unpublished). Therefore, the atomic mixing length at the interface, $(\Delta z)_{\text{mix}}$, is given by:

$$(\Delta z)^2_{\text{mix}} = (\Delta z)^2_{\text{meas}} - (\Delta z)^2_{\text{corr}} \quad (3)$$

where $(\Delta z)_{\text{meas}}$ and $(\Delta z)_{\text{corr}}$ are the measured interface length (as provided by the depth profile) and the RMS roughness of the interface. In addition, the measured interface length is considered to be the distance between the normalized yields of two markers representative of the films that make up the interface taken at the 10% level of their maximum. A word of caution needs to be expressed here: atomic mixing and roughness cannot be completely disentangled. Within the MRI model one needs to define clearly the roughness such that it is completely separated from atomic mixing. In our case, we define the roughness as the RMS roughness given by a tool that can provide surface topography with nanometer resolution (i.e., AFM).

2.3 Results and Discussion

Figure 2.1 depicts plan-view SEM images of Cu surfaces after 250 to 3000 ALD cycles (~1 to 16 nm films assuming conformal coverage and extrapolating from cross-sectional TEM images of thicker 1000- and 3000-cycle films in Figure 2.2). The SEM images illustrate that minimal 3D faceting is evident after 250 cycles (Figure 2.2A). By 500 cycles (2.3 nm Co), 3D faceting of the Co surface is apparent in SEM and is effectively

unchanged up to 1000 cycles (4.5 nm, Figures 2.2B and 2.2C, respectively). From 250 to 1000 cycles, the relative Co:Cu atomic ratio detected in XPS increases from 3.3 to 26.5 and doubles from 500 to 1000 ALD cycles and again from 1000 to 3000 cycles giving a final Co:Cu atomic ratio of 49.8. Although the surface faceting is indistinguishable between 500 and 1000 cycles, the increasing Co:Cu ratio suggests that the film thickens or increases in density with little surface modification. By 3000 cycles, the Co film surface appears polygranular and multifaceted (Figure 2.2D).

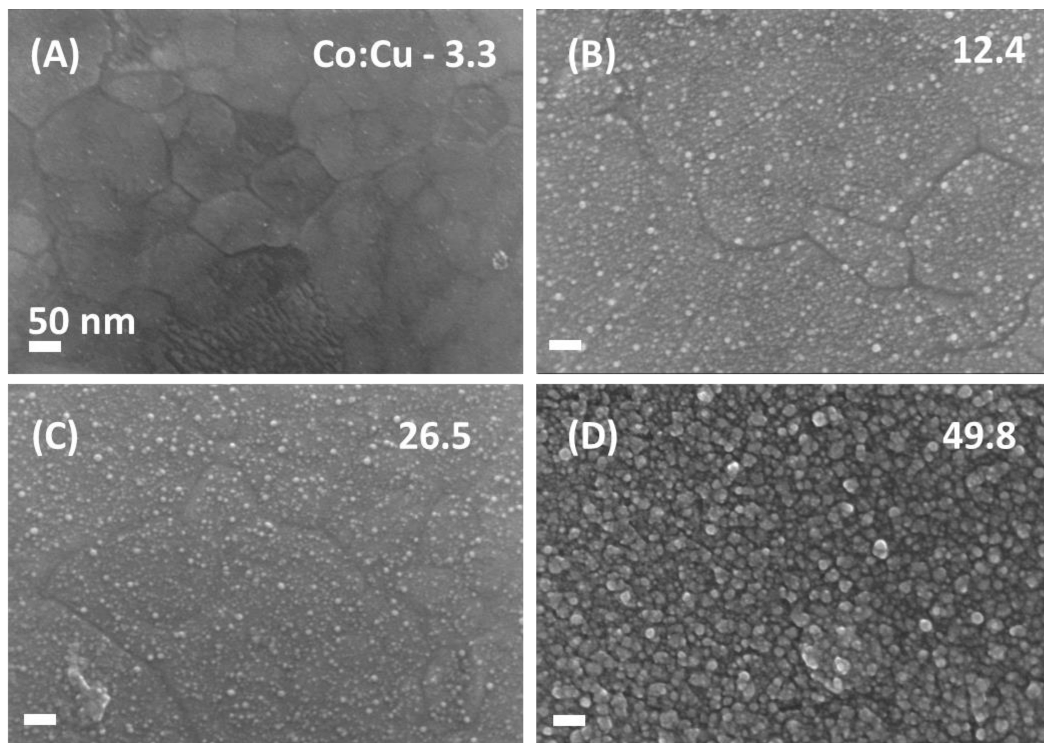

Figure 2.1. Plan-view SEM images of (A) 250, (B) 500, (C) 1000, and (D) 3000 cycle ALD depositions of CoAMD on Cu at 265 °C. The calibrated Co:Cu atomic ratio detected in XPS is listed in the upper right-hand corner of each figure.

Figure 2.2 presents AFM and cross-sectional TEM data from 1000- and 3000-cycle Co films. The TEM images indicate that the Co films are continuous and polygranular. The

1000- and 3000-cycle films, 4.5 and 16 nm thick, exhibit RMS roughnesses of 1.9 and 4.8 nm, respectively.

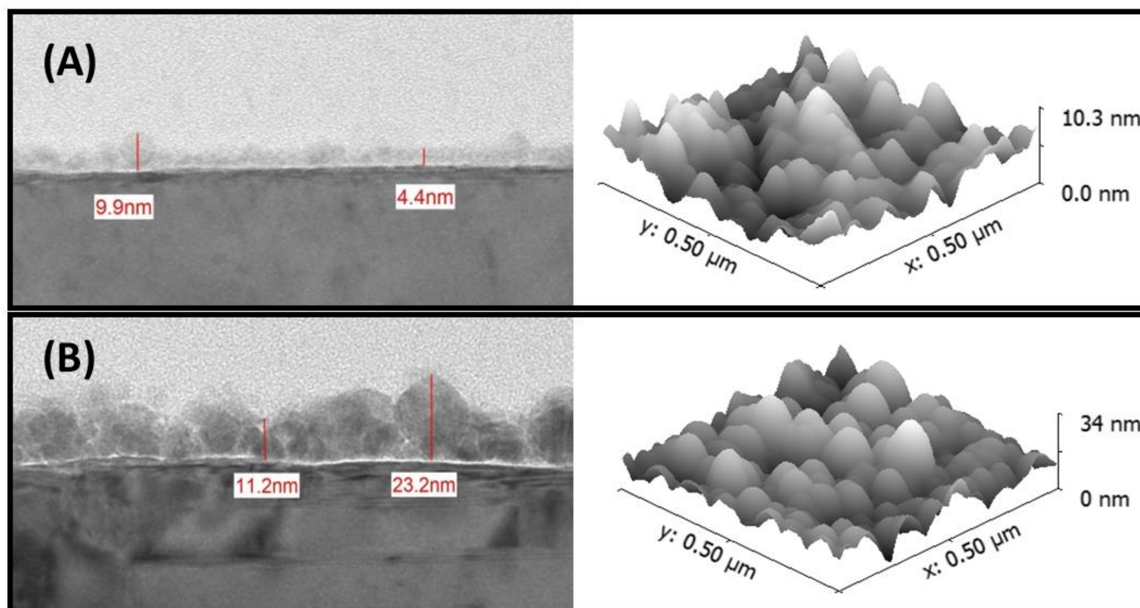

Figure 2.2. Cross-sectional TEM images and surface topography renderings from AFM of (A) 1000 cycle and (B) 3000 cycle ALD of CoAMD on Cu at 265 °C.

Figure 2.3 presents normalized ToF-SIMS spectra of the 1000- and 3000-cycle films. From Figures 2.3A and 2.3B it is apparent that for both films a finite amount of Cu is segregated to the films' free surfaces and that Cu is detected throughout the Co films as indicated by the black CuO^- trace. A Co rich layer is observed preceding the Co/Cu mixing region after which only bulk Cu is detected. For the 3000-cycle film, a local minimum of Cu concentration occurs between the surface-segregated Cu and the Cu that diffused into the Co film between 8 and 12 nm depth. The extent of the Co/Cu intermixing region is indicated in Figures 2.3A and 2.3B and is 3.6 nm for the 1000-cycle film and 10.2 nm for the 3000-cycle film as determined by the MRI model (supporting information). Figures 2.3C and 2.3D present more comprehensive ToF-SIMS profiles. Simplified schematics of

the relevant species in order of appearance during depth profiling are depicted in the insets. The insets in Figures 2.3C and 2.3D describe the sample as measured after storage in air before *ex situ* analysis by ToF-SIMS. Oxides of the film elements are due to *ex situ* storage before ToF-SIMS depth profiling. *In situ* XP spectra of the as deposited films show no O contamination of Co (Figure 2.4).

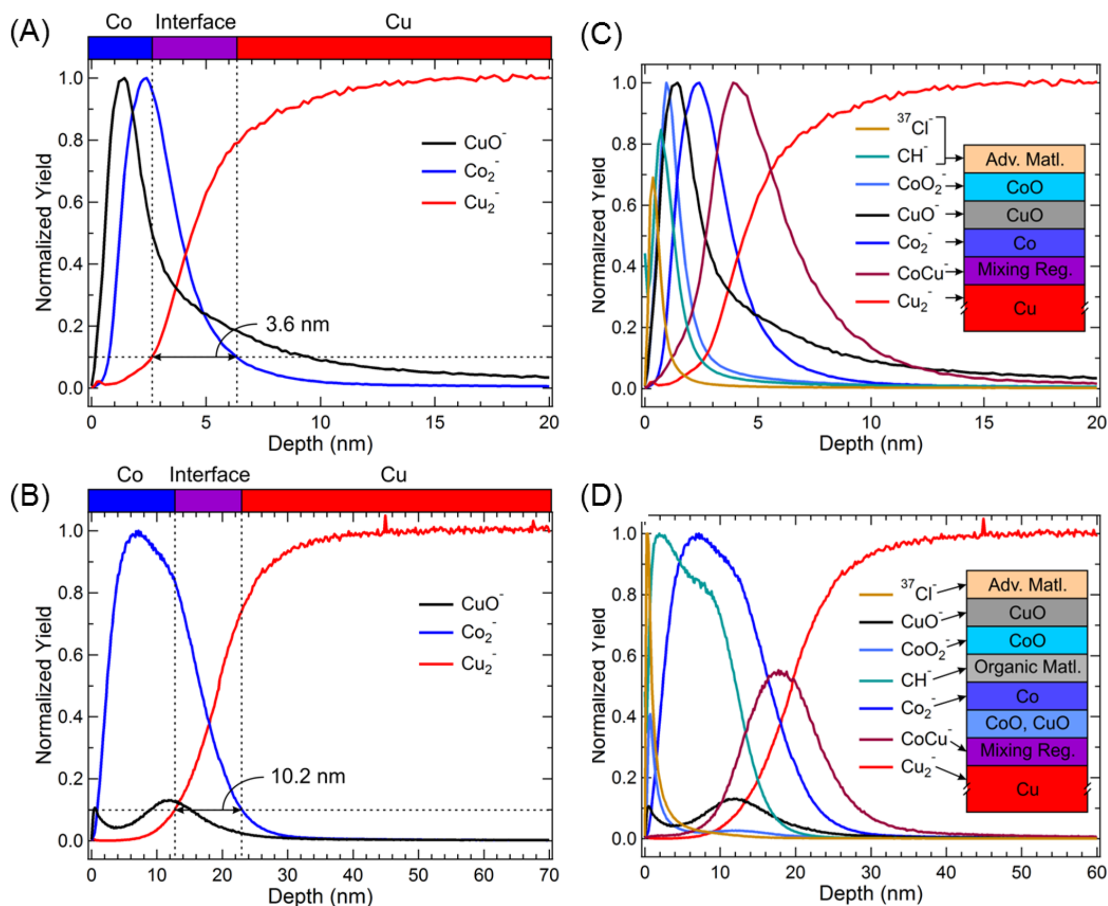

Figure 2.3. ToF-SIMS depth profiles of 1000 cyc Co film: (A) and (C), and 3000 cycle Co film: (B) and (D). Adv. Matl. refers to adventitious material accumulated on the substrate during sample storage and after air transfer for analysis and was not present *in situ* following deposition.

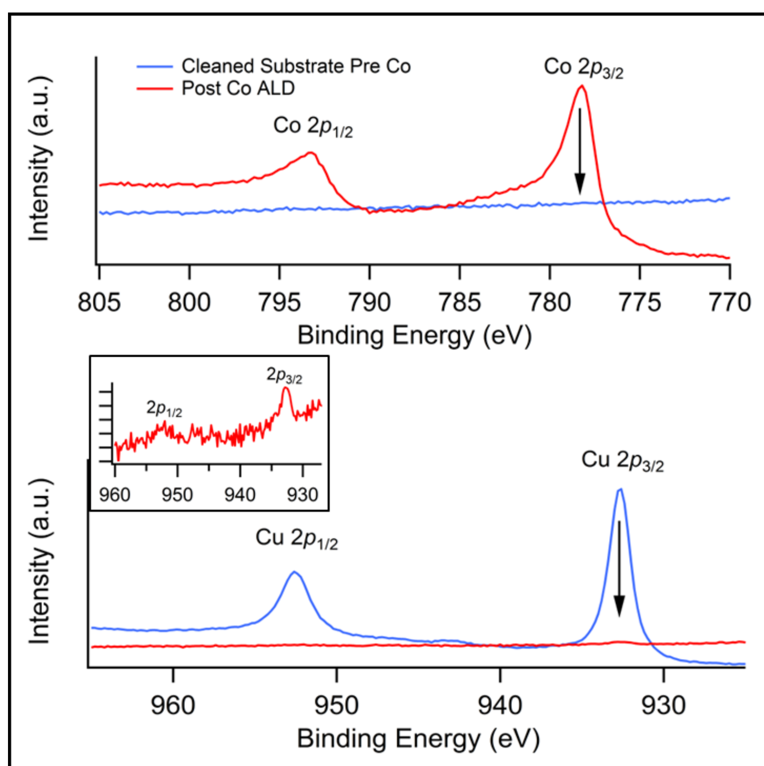

Figure 2.4. As deposited Co (top) and Cu (bottom) 2*p* X-ray photoelectron spectra from a 16 nm (3000 ALD cycle from CoAMD) Co film on Cu substrate. The reduced Co^0 and Cu^0 positions are depicted by arrows at the $2p_{3/2}$ peaks, 778.3 eV and 932.7 eV, respectively. Some Cu signal is still apparent in XPS after Co deposition as indicated by the Cu 2*p* inset.

Figure 2.5 is a schematic representation of Co film growth from CoAMD on Cu. The as-deposited Co films generally comprise a Co-rich, polycrystalline layer with a thin Cu surface coating and are free from oxidation. Co film growth on Cu proceeds first by the formation of a 2D wetting film and intermixing layer of Co and Cu. Cu is observed to segregate to the surface of the accumulating Co film in order to minimize the free surface energy [18]. The surfactant-like behavior that maintains Cu concentration at the uppermost layer of the Co film as it deposits suggests that Cu may stabilize the first several monolayers of Co leading to a wetting film [3]. Venables previously described a phenomenon by which higher energy overlayers burrow into lower energy surfaces and become coated in a thin

layer of the lower energy substrate [19]. This occurs especially during the deposition of magnetic materials on more noble metal substrates [16,17]. Moreover, Li and Tonner have demonstrated that annealing Co fcc films grown epitaxially on Cu (001) to 400 °C induced a thin layer of Cu to migrate to the Co free surface [21]. They suggested that Cu atoms undergo an inversion process by which Cu substrate atoms segregated to the surface of the Co film to act as a stabilizing layer for the mismatched Co film.

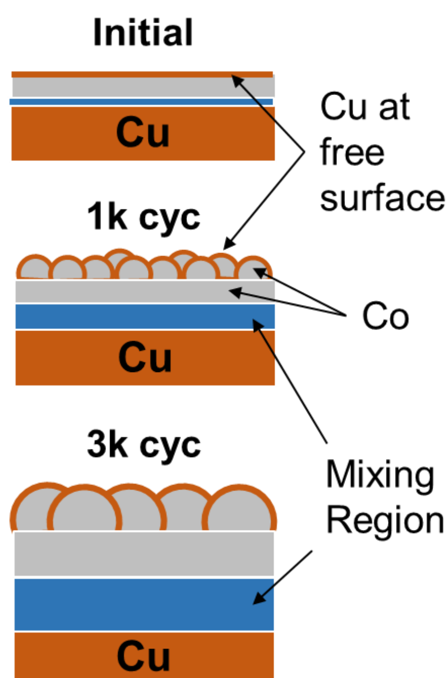

Figure 2.5. Growth mode of Co films on Cu by ALD from CoAMD.

Once the Co-rich layer is thick enough, 3D faceting of the Co begins. The apparent transition from 2D to 3D growth may reflect preferential deposition at grains of a specific crystallographic orientation or reconciliation of heteroepitaxial strain between the Co, for which bulk films prepared below 420 - 450 °C are generally hcp, and Cu for which an fcc structure is more stable [6,9,19,20].

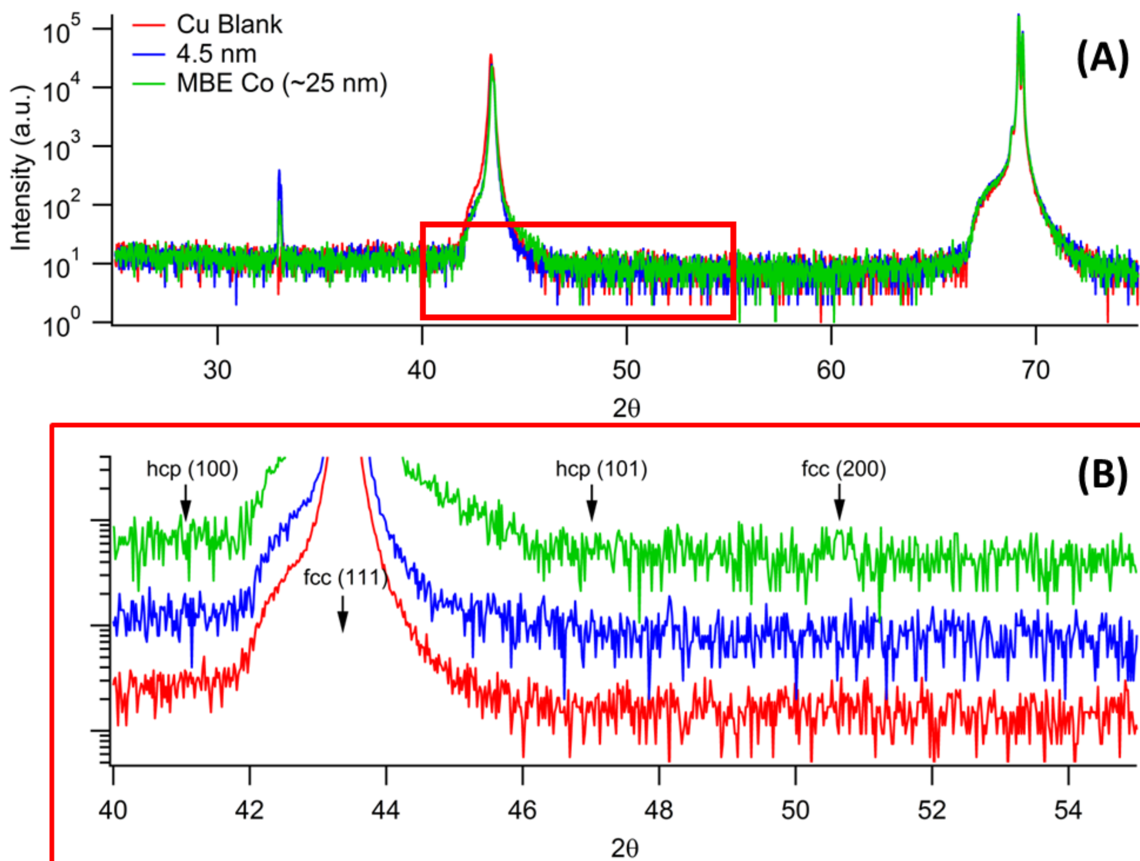

Figure 2.6. XRD data from Co films on Cu. (A) depicts the raw signal for a blank Cu substrate, 300 nm on Si, a 5 nm, 1000 ALD cycle Co film from CoAMD deposited at T_s: 265 °C, and a molecular beam epitaxy-deposited Co film on the same Cu substrate held at T_s: 265 °C. (B) depicts the inset from (A), boxed in red, and highlights the relevant XRD signals for the Co films. The fcc (111) signal may include information from Cu and Co from which the Co signal cannot be isolated. Further, hcp (100) and hcp (101) Co signals are not observed after ALD or MBE but are often indiscernible from the signal noise in sub-40 nm films [24]. A faint fcc (200) signal is apparent for the MBE sample.

The crystalline structure of the Co is likely a mixture of fcc and hcp Co. X-ray diffraction studies revealed strong fcc (111) signals for blank Cu wafers and 4.5 nm Co/Cu film samples (Figure 2.6). However, distinct hcp signals were indiscernible from the signal

noise if present and the Co contribution to the fcc signal is inseparable from the Cu contribution due to the magnitude of the signal. A thicker (~25 nm) Co film was deposited by molecular beam epitaxy but revealed only a very weak fcc (200) signal in additional to those observed on blank Cu. Efforts by Deo *et al.* suggest that even very thick Co films (~ 200 nm) exhibit small XRD signals and that data from Co films less than 40 nm thick are clouded by noise [24]. It is, therefore, reasonable to expect that hcp signals from the 4.5 nm and 25 nm films are too small to observe. Nevertheless, evidence of pseudoepitaxial Co/Cu layers in superlattices formed by fcc/hcp stacking faults fit well with our Co film behavior [6,7].

2.4 CONCLUSIONS

In summary, Co deposition by ALD from CoAMD proceeds first by a metastable 2D Co-rich layer that grows on the Cu substrate until enough Co is deposited that the film begins to roughen and grow three dimensionally. The Co-rich layer remains while Co continues to accumulate as indicated by ToF-SIMS depth profiling. Further, a surfactant-like Cu layer is apparent on the surface of the Co up to at least 16 nm film thicknesses suggesting that the Cu plays a role in the Co deposition and may stabilize the Co film especially at the early stages of film deposition. The Cu surface layer may improve Co lattice matching as pseudoepitaxial fcc and hcp Co grains can be expected on the Cu surface. Finally, highly mobile Cu and Co at the film interface leads to significant intermixing of the species during Co deposition even at 265 °C as well as grain boundary diffusion of Cu through the Co film.

2.5 REFERENCES

[1] P. Moon, V. Dubin, S. Johnston, J. Leu, K. Raol, and C. Wu, "Process Roadmap and Challenges for Metal Barriers," *IEEE - IEDM*, no. C, pp. 841–844, 2003.

[2] R. G. Gordon, H. Kim, and H. Bhandari, "Cobalt Nitride Layers for Copper Interconnects and Methods for Forming Them," US 7,973,789 B22011.

[3] A. Kohn, M. Eizenberg, and Y. Shacham-Diamand, "Copper grain boundary diffusion in electroless deposited cobalt based films and its influence on diffusion barrier integrity for copper metallization," *J. Appl. Phys.*, vol. 94, no. 5, p. 3015, 2003.

[4] C. S. Hau-Riege, "An introduction to Cu electromigration," *Microelectron. Reliab.*, vol. 44, no. 2, pp. 195–205, Feb. 2004.

[5] "International Technology Roadmap for Semiconductors - Interconnect," 2011.

[6] B. P. Tonner, Z.-L. Han, and J. Zhang, "Structure of Co films grown on Cu(111) studied by photoelectron diffraction," *Phys. Rev. B*, vol. 47, no. 15, pp. 9723–9732, 1993.

[7] F. J. Lamelas, C. H. Lee, H. He, W. Vavra, and R. Clarke, "Coherent fcc stacking in epitaxial Co/Cu superlattices," *Phys. Rev. B*, vol. 40, no. 8, pp. 5837–5840, 1989.

[8] L. Zhang, M. Kraatz, O. Aubel, C. Hennesthal, J. Im, E. Zschech, and P. S. Ho, "Cap layer and grain size effects on electromigration reliability in Cu/low-k interconnects," *2010 IEEE Int. Interconnect Technol. Conf.*, pp. 1–3, Jun. 2010.

[9] H. Shimizu, K. Sakoda, T. Momose, and Y. Shimogaki, "Atomic Layer Deposited Co(W) Film as a Single-Layered Barrier/Liner for Next-Generation Cu-Interconnects," *Jpn. J. Appl. Phys.*, vol. 51, p. 05EB02, May 2012.

[10] C.-C. Yang, P. Flaitz, P.-C. Wang, F. Chen, and D. Edelstein, "Characterization of Selectively Deposited Cobalt Capping Layers: Selectivity and Electromigration Resistance," *IEEE Electron Device Lett.*, vol. 31, no. 7, pp. 728–730, Jul. 2010.

[11] M. F. Chioncel and P. W. Haycock, "Structural Characterization of Cobalt Thin Films Grown by Metal-Organic CVD," *Chem. Vap. Depos.*, vol. 11, no. 5, pp. 235–243, May 2005.

[12] B. S. Lim, A. Rahtu, and R. G. Gordon, "Atomic layer deposition of transition metals.," *Nat. Mater.*, vol. 2, no. 11, pp. 749–754, Nov. 2003.

[13] H. B. Bhandari, J. Yang, H. Kim, Y. Lin, R. G. Gordon, Q. M. Wang, J.-S. M. Lehn, H. Li, and D. Shenai, "Chemical Vapor Deposition of Cobalt Nitride and its Application as an Adhesion-Enhancing Layer for Advanced Copper Interconnects," *ECS J. Solid State Sci. Technol.*, vol. 1, no. 5, pp. N79–N84, Sep. 2012.

[14] T. D. M. Elko-Hansen and J. G. Ekerdt, "XPS investigation of the atomic layer deposition half reactions of bis (N-tert-butyl-N ' -ethylpropionamidinato) cobalt (II)." Austin, 2014.

[15] J. D. Zimmerman, B. E. Lassiter, X. Xiao, K. Sun, A. Dolocan, R. Gearba, D. a Vanden Bout, K. J. Stevenson, P. Wickramasinghe, M. E. Thompson, and S. R. Forrest, "Control of interface order by inverse quasi-epitaxial growth of squaraine/fullerene thin film photovoltaics.," *ACS Nano*, vol. 7, no. 10, pp. 9268–75, Oct. 2013.

[16] S. Hofmann, "Sputter depth profile analysis of interfaces," *Reports Prog. Phys.*, vol. 61, pp. 827–888, 1998.

[17] S. Hofmann, "Profile reconstruction in sputter depth profiling," *Thin Solid Films*, vol. 398–399, pp. 336–342, Nov. 2001.

[18] L. Vitos, A. V Ruban, H. L. Skriver, and J. Kolla, "The surface energy of metals," *Surf. Sci.*, vol. 411, pp. 186–202, 1998.

[19] J. A. Venables, *Introduction to Surface and Thin Film Processes*. New York, NY: Cambridge University Press, 2000.

[20] A. Christensen, A. V Ruban, P. Stoltze, K. W. Jacobsen, H. L. Skriver, J. K. No, and F. Besenbacher, "Phase diagrams for surface alloys," vol. 56, no. 10, pp. 5822–5834, 1997.

[21] H. Li and B. P. Tonner, "Structure and growth mode of metastable fcc cobalt ultrathin films on Cu (001) as determined by angle-resolved X-ray photoemission scattering," *Surf. Sci.*, vol. 237, pp. 141–152, 1990.

[22] O. Nilsen, O. B. Karlsen, A. Kjekshus, and H. Fjellvåg, "Simulation of growth dynamics for nearly epitaxial films," *J. Cryst. Growth*, vol. 308, no. 2, pp. 366–375, Oct. 2007.

[23] O. Nilsen, O. B. Karlsen, A. Kjekshus, and H. Fjellvåg, "Simulation of growth dynamics in atomic layer deposition. Part I. Amorphous films," *Thin Solid Films*, vol. 515, no. 11, pp. 4527–4537, Apr. 2007.

[24] N. Deo, M. F. Bain, J. H. Montgomery, and H. S. Gamble, "Study of magnetic properties of thin cobalt films deposited by chemical vapour deposition," *J. Mater. Sci. Mater. Electron.*, vol. 16, no. 7, pp. 387–392, Jul. 2005.

Chapter 3: Selectivity-enhanced Atomic Layer Deposition of Co on Cu relative to SiO_2 and Carbon Doped Oxide Dielectrics

3.1 INTRODUCTION

The scaling of microelectronics necessitates further mitigation of Cu electromigration (EM). Cu EM in back end of line (BEOL) Cu interconnects leads to premature device failure and is exacerbated by higher current densities in the increasingly smaller metallization lines [1,2]. Co metal caps have proven effective at inhibiting Cu EM [1,3]. While Co can be deposited by a variety of processes including physical vapor deposition (PVD) and electroless deposition, vapor delivery processes, particularly area-selective atomic layer deposition (AS-ALD), demonstrate great promise. AS-ALD improves on physical deposition methods by depositing ultrathin, highly conformal films while avoiding costly photolithography patterning processes. Avoiding extensive post-processing for PVD films and removing contamination from the electroless deposition bath also allows for greater wafer throughput.

Good-quality AS-ALD for BEOL materials requires highly controllable, reductant-activated ALD precursors with adequate vapor pressure. The precursor should have a wide ALD temperature range and little CVD behavior to mitigate deposition on the adjacent interlayer dielectric (ILD). Furthermore, high-temperature ALD processes should be avoided to minimize the thermal budget of the device. It has been demonstrated that amidinate-based Co complexes are effective ALD precursors using either H_2 or NH_3 coreactant. In particular, Bis(*N,N'*-diisopropylacetamidinato)cobalt(II) (Co-iPrAMD) and bis(*N*-tert-butyl-*N'*-ethylpropionamidinato) cobalt(II) (CoAMD) are commercially available from Dow and have been used for ALD and CVD processes [1–4]. However, appreciable deposition rates for Co-iPrAMD have not been reported for temperatures less

than 300 °C [8]. We have previously demonstrated self-limiting ALD of Co on Cu from CoAMD using H_2 as the coreactant [9].

To achieve complete selectivity, it is also necessary to passivate the ILD surfaces. In particular, O-containing surface moieties, *e.g.*, OH terminations, have been demonstrated as favorable chemisorption sites for many ALD precursors, including Co amidinates [10]. Self-assembled monolayers and liquid passivant treatments of ILD materials are demonstrated in the literature however vapor-delivered passivants offer simpler scalability [7, 8]. Silane-based passivant chemistries are widely demonstrated on SiO_2 surfaces and favor vapor delivery [13]. The effect of these passivants on low-k dielectrics like carbon-doped oxide, however, is not well known. CDO shares the Si-O backbone of SiO_2 but also comprises a large amount of C. Many surface terminations are $–CH_3$ or –H rather than O containing moieties like –OH. Further, depending on the surface pretreatment, Si from the SiO_2 backbone may be terminated by -H in the case of acid etch, -OH for basic etches such as tetra-methyl ammonium hydroxide, or –OOH for carboxylic acid treatments. The surface terminations of CDO and SiO_2 determine what passivation strategies will be most effective. In this work, CDO and SiO_2 are cleaned to yield maximum –OH termination. Therefore, passivants that target –OH groups, Trimethyl chlorosilane (TMCS), hexamethyl disilizane (HMDS), and BDMAS, were evaluated for their passivation of CDO and SiO_2 surfaces. This study demonstrates dielectric-surface-passivation-enhanced area-selective ALD of Co capping layers from CoAMD on BEOL Cu interconnects.

3.2 Experimental Methods

Initial passivation studies were performed on blanket Cu (300 nm PVD on Si), CDO (k ~ 2.6), and SiO_2 (6kA thermal oxide) that were provided by Intel. Growths were also performed on Intel provided patterned wafers for cross-sectional transmission electron

microscopy (TEM). AccuDep® CoAMD was supplied by Dow Chemical. Coreactant H_2 and Ar sweep gases were provided by Matheson (99.999%). The as-received substrates were cleaned by rinsing in order with acetone, ethanol (Fisher ACS grade), and deionized (DI) water (18MΩ). Following the rinse, Cu substrates were cleaned of the majority of the surface oxide by one min soaks in 35 °C glacial acetic acid (99.9%, Fisher Scientific) [14]. SiO_2 samples were placed in a piranha bath (6:2:1 - H_2SO_4 (Fisher ACS plus) : H_2O_2 (Fisher 30%) : DI H_2O) for 15 min followed by a 10 s HF (2%) etch. CDO was cleaned in a 1:1:1 tetramethylammoniumhydroxide (Acros Organics 25% in water) : ethylene glycol (Fisher) : DI H_2O bath for 2 min at 50 °C.

Cleaned samples were transferred via load lock into a previously described, in-house built ALD system [Tuo]. The ALD system comprises *in situ* transfer between a hot-walled ALD growth chamber, a characterization chamber, a chemical titration chamber, and a thermal evaporation source for metals deposition. The characterization chamber houses an X-ray photoelectron spectrometer (PHI model 1600) with Ar^+ sputtering capabilities.

Co depositions were performed in the ALD chamber. In the ALD chamber, substrates are held perpendicularly to the flow of precursor gases carried by an Ar sweep. Substrate temperature is measured by K-type thermocouple just below the substrate. ALD operating pressure is 260mTorr. A typical ALD cycle comprises alternating 2s CoAMD exposures, corresponding to ~7×10^5 L (1L = 1×10^{-6} torr×s), and 15 s H_2 coreactant exposures (1.0×10^7 L) separated by 15 s Ar purges (5.4×10^6 L). ALD cycling was consistent for all Co deposition experiments and only the number of cycles and, in the case of the temperature dependence tests, temperature were varied.

Surface passivations were performed *in situ* in the passivation chamber. The passivation chamber is a hot-wall chamber controlled by constant power input and sample

temperatures are measured on the stage immediately below the sample holder. Substrate surface temperature differs by < 5 °C from the measured temperature, typically 50 °C unless otherwise specified. Passivations were performed by delivering a set pressure of passivant vapor, determined by the vapor pressure of the passivant at its delivery temperature, for a set amount of time and is reported as Torr-s (the product of the pressure and exposure time). For exposures less than 50 kTorr-s, typical passivation pressures were ~ 8 Torr. For extended exposures, greater than or equal to 50 kTorr-s, pressures of ~60 Torr were used. During extended exposures a moderate substrate temperature increase of less than 10 °C occurred as the heating was power, not temperature controlled. After a passivation exposure the chamber was evacuated and the sample transferred to the ALD chamber in which it was annealed to a substrate surface temperature of 265 °C under 50 sccm H_2 and 50 sccm Ar flow to clear adsorbed surface species. Most samples were transferred *in situ* for X-ray photoelectron spectroscopy (XPS) measurements after annealing but before Co deposition. Control studies indicated that this transfer to and from the XPS before Co deposition did not affect the Co accumulation after passivation.

3.3 Results and Discussion

SiO_2 and CDO substrate surfaces share a backbone network of Si and O. While the C content of CDO reduces the amount of surface O sites, because O and OH surfaces species are the primary reactive surface species, similar passivation methods may be employed for SiO_2 and CDO [10,15]. In this work, the surface OH species that result from substrate cleaning are targeted for chemical passivation. The freshly cleaned samples are exposed to a silane-based passivant before undergoing ALD with CoAMD and H_2. The passivated, post-ALD surfaces are evaluated for improvements in selectivity by *in situ* XPS. Figure 3.1 provides a schematic for the general passivation methodology of this work.

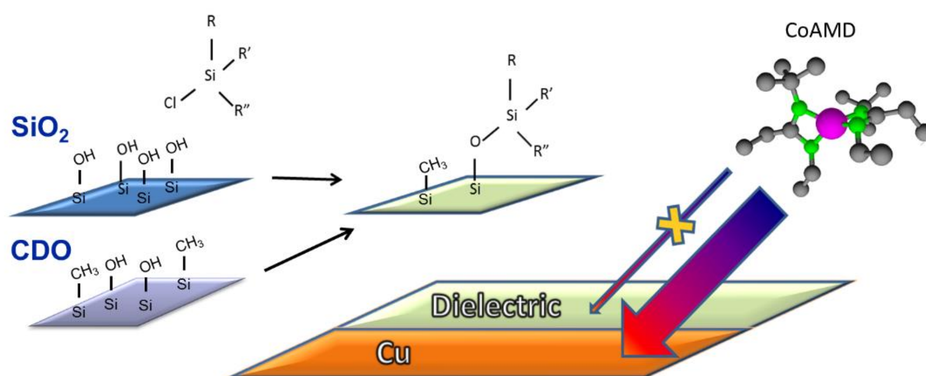

Figure 3.1. Schematic for OH targeting passivation scheme.

Preliminary passivant evaluations were performed to establish whether the passivation inhibited nucleation during the first few ALD cycles. Substrates were exposed the BDMAS, HMDS, or TMCS and then annealed in a reducing H_2 atmosphere to remove physisorbed passivant and clear any remaining products of the passivation reaction. Substrates were then exposed to three ALD cycles of CoAMD and H_2 at 265 °C. The Co accumulated on each substrate is normalized to the amount of Co present after three ALD cycles on the respective, untreated substrates and is presented in Figure 3.2. BDMAS and HMDS exposure decreased Co accumulation on all three substrates for 3 kTorr-s exposures at 50 °C. HMDS, in particular, negatively impacted Co accumulation on the Cu substrate. 50 Torr-s TMCS exposure at 50 °C decreased accumulation on SiO_2 and CDO by 45% and 80%, respectively. Accumulation on Cu was only reduced by 25% relative to untreated Cu. In all cases, the total exposure time for HMDS and BDMAS exceeded TMCS by two orders of magnitude to achieve the same Cu to CDO selectivity. Further, the data indicate that while HMDS was most effective at inhibiting nucleation on SiO_2 relative to Cu, TMCS was the most effective passivant for CDO. While SiO_2 and CDO both exhibit surface OH species and siloxane bridges, it is apparent that their interactions with the passivants differ. From this test, it was determined that TMCS was the most likely candidate to enhance

CoAMD selectivity for Cu over the CDO substrates. BDMAS was eliminated entirely as it was the least effective passivant in the preliminary tests.

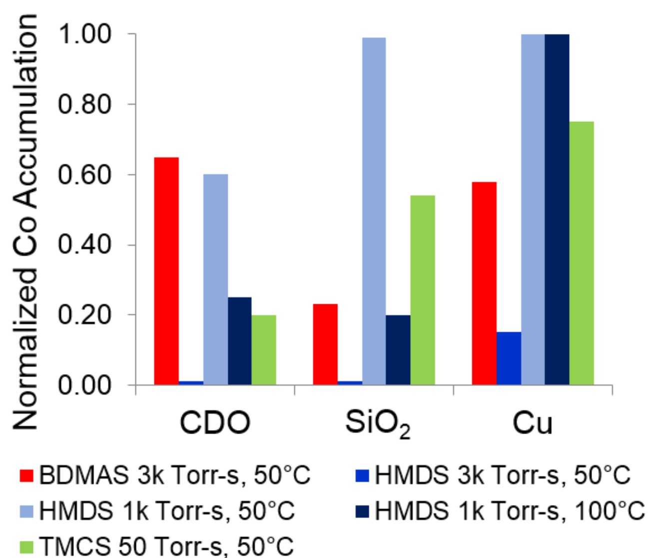

Figure 3.2. XPS measured Co atomic percentages accumulated after 3×2s adsorption of CoAMD at 265 °C on passivant treated Cu, SiO_2, and CDO substrates. Co accumulation is normalized for each substrate relative to their respective Co accumulation with no surface passivation. Passivant treatments are listed in the figure legend.

To evaluate the efficacy of the passivants under thin-film deposition conditions, 250 cycles of CoAMD was deposited at 265 °C on each substrate after passivation (Figure 3.3). Under these conditions, 1 kTorr-s HMDS exposure proved ineffective and did not reduce Co accumulation at all on CDO or Cu, although accumulation on SiO_2 was reduced by 25%. The 3 kTorr-s BDMAS exposure proved more effective and reduced accumulation on CDO, SiO_2, and Cu by 48%, 85%, and 25%, respectively. In this set of experiments, TMCS was again the best at improving selectivity for Cu over CDO. Accumulation after 50 Torr-s TMCS exposure at 50 °C was reduced by 60% on CDO and 25% on Cu. At these conditions, TMCS exposure did not reduce accumulation on SiO_2 significantly.

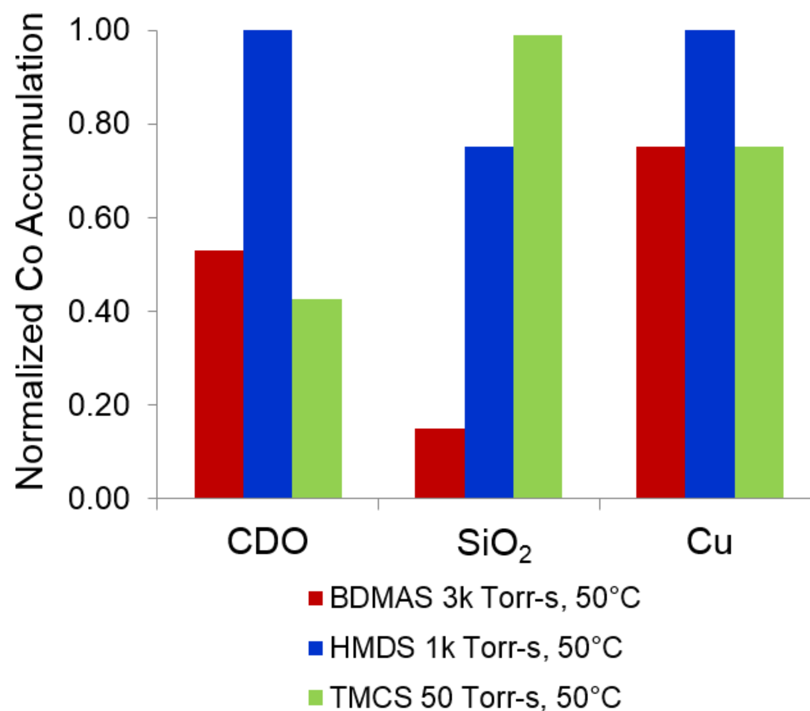

Figure 3.3. Co accumulation after 250 ALD-cycle deposition of CoAMD at 265 °C on passivant treated Cu, SiO_2, and CDO substrates. Co accumulation is normalized for each substrate relative to their respective Co accumulation with no surface passivation. Passivant treatments are listed in the figure legend.

To enable selectivity it is also important to avoid thermal decomposition of the precursor on the substrate, *i.e.*, employ a temperature range that maximizes ALD behavior. Co 2*p* XP spectra indicate that when inert polyimide and Teflon substrates underwent 250 cycle exposures to CoAMD at 265 °C Co accumulated appreciably on both substrates (Figure 3.4). Although ALD of this CoAMD has been generally reported at temperatures exceeding 250 °C [4], it is apparent that some thermal decomposition of CoAMD occurs

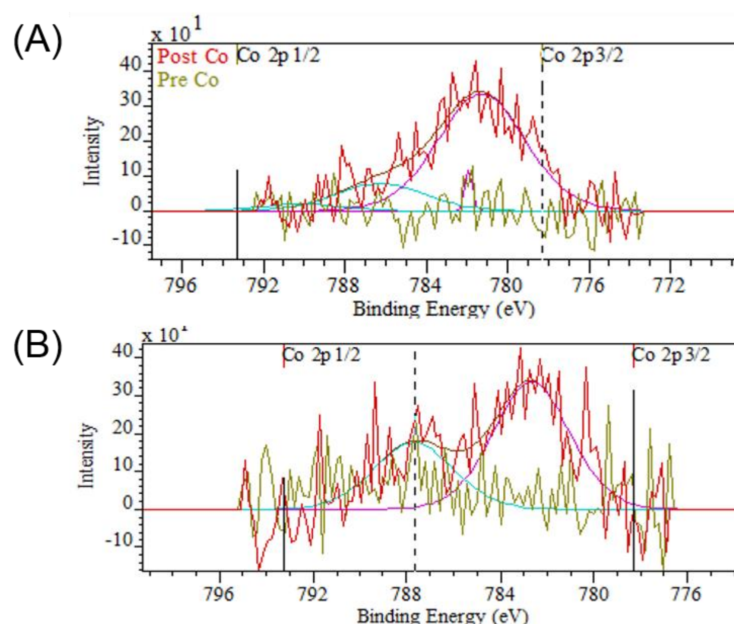

Figure 3.4. Co 2p XP spectra of Co accumulation after 250 ALD-cycle deposition of CoAMD at 265 °C on inert (A) polyimide and (B) Teflon surfaces.

at elevated temperatures. Further, once Co is nucleated on CDO, CoAMD will continue to dissociate on Co surface clusters. To maintain selectivity, the initial nucleation of Co on CDO must be avoided. In order to leverage the inherent selective of CoAMD for Cu and avoid Co deposition on CDO from thermal decomposition, 50 ALD-cycle depositions were performed on CDO and Cu for temperatures between 165 and 265 °C were performed to evaluate the optimum deposition temperature for enhanced surface selectivity (Figure 3.5). For Cu, Co accumulation is nearly the same from 165 to 265 °C, 12-14 atomic percent with ~ 1% standard deviation. Co accumulation on CDO, however, is highly temperature dependent above 190 °C. Decreasing the deposition temperature from 265 °C to 165 °C decreased Co accumulation on CDO after 50 cycles by two times. Moreover, at 265 °C, Co preferentially deposits three to one on Cu versus CDO. At 165 °C, the preference for Cu becomes nearly five to one before any passivation. Therefore, to fully leverage the inherent surface selectivity of CoAMD, ALD may be performed at temperatures as low as

165 °C. It is important to note that reducing the temperature also affects the desorption from or subsequent reaction of AMD ligands on the substrate surfaces.

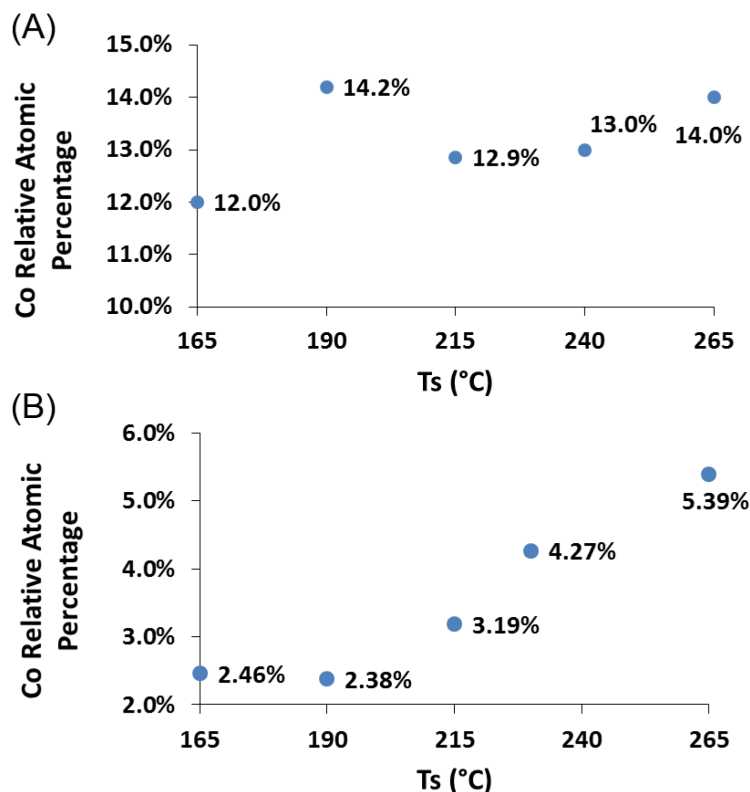

Figure 3.5. XPS derived Co atomic percentage accumulation on untreated Cu and CDO after 50 ALD cycles of CoAMD with H_2 at various temperatures.

Many precursors already suffer from relatively high C incorporation and we have previously reported Co films deposited on Cu from CoAMD containing C atomic concentrations around 18% [9].

By leveraging the disparity in deposition rate of Co on Cu relative to CDO and employing OH targeting passivation chemistries, the chemical surface selectivity of CoAMD can be increased significantly. Specifically, for depositions at 165 °C

pretreatments of 50 and 500 kTorr-s of TMCS at 50 °C (not shown) decreased the relative atomic percent of Co from 2.46% on untreated CDO to 1% and 0.4%, respectively. On Cu, Co deposition was unaffected by the passivation treatment. For 500 kTorr-s TMCS exposure a 30:1 deposition preference of CoAMD for Cu versus CDO was observed for 50 cycle ALD depositions.

Patterned line-spaced wafers (LSW) from Intel were used to test the effects of low temperature ALD and TMCS passivation for selective Co deposition on Cu interconnect lines. To remove surface oxide on the Cu lines, LSWs were dipped once in glacial acetic acid (1 min at 35 °C). Cross-sectional TEM images were obtained for 500 and 1000 cycle Co films (2.4 and 3 nm thick, respectively) deposited at 165 °C after 50 kTorr-s TMCS passivation at 50 °C (Figures 3.6 A and B, respectively). A thin, continuous Co film is discernible on each Cu interconnect while no Co is apparent on the Cu-ILD barrier. For the 500-cycle film, a small amount of discontinuous Co is visible on the ILD. Co contamination on the 1000 cycle film ILD is more pronounced. In separate experiments (not shown) CDO blanket substrates were exposed to the same acetic acid treatment and 50 ALD cycles of CoAMD at 165 °C. After acetic acid treatment, the blanket CDO wafers exhibited greater Co accumulation than TMAH cleaned or uncleaned CDO substrates. Further, passivating acetic acid treated CDO with 50 kTorr-s TMCS did reduce Co accumulation but the Co atomic concentration remained greater than 2.45% expected on CDO with no treatment. Therefore, the Co accumulation on the ILD in Figure 3.6 is greater than would be expected from patterned metallization layers that are processed *in situ* without the necessary cleaning steps performed in this work to remove oxidized Cu surface layers.

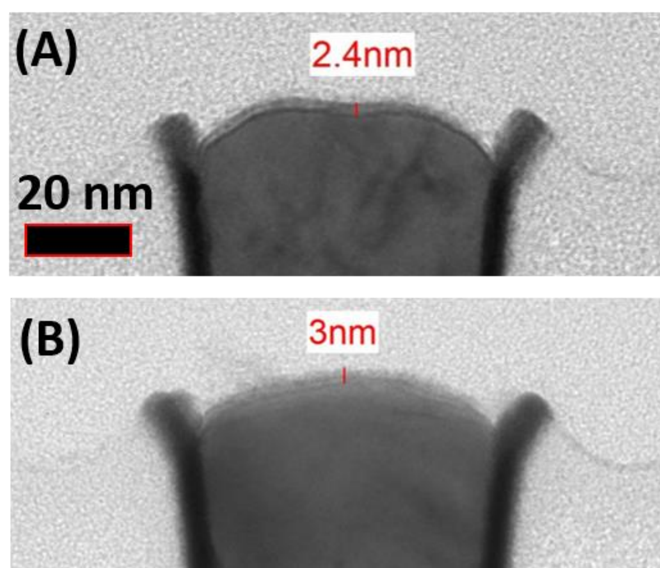

Figure 3.6. Cross-sectional TEM images of Co accumulation on TMCS (50 kTorr-s at 50 °C) treated, acetic acid etched LSW substrates. (A) 500 cycle and (B) 1000 cycle Co ALD at 165 °C.

3.4 Conclusions

In summary, enhanced surface selectivity for Co capping layers can be achieved using a surface selecting precursor, CoAMD, and by leveraging low-temperature ALD and surface chemical passivation. This scheme for selectivity is all vapor-delivery based, making it highly scalable. Further, given pristine samples with no air transfer, the selectivity of CoAMD for Cu over passivated CDO is expected to increase and complete inhibition of nucleation on the ILD should be possible.

3.5 References

[1] R. G. Filippi, P.-C. Wang, a. Brendler, K. Chanda, and J. R. Lloyd, "Implications of a threshold failure time and void nucleation on electromigration of copper interconnects," *J. Appl. Phys.*, vol. 107, no. 10, p. 103709, 2010.

[2] M. Hauschildt, M. Gall, P. Justison, R. Hernandez, M. Herrick, S. Ogawa, P. S. Ho, and E. Zschech, "Large-Scale Statistical Study of Electromigration Early Failure for Cu/low-k Interconnects," *AIP Conf. Proc.*, vol. 945, pp. 66–81, 2007.

[3] T. Kirimura, K. Croes, Y. K. Siew, K. Vanstreels, P. Czarnecki, Z. El-mekki, M. H. Van Der Veen, D. Dictus, A. Yoon, A. Kolics, J. Bömmels, and Z. Tőkei, "Void nucleation and growth during electromigration in 30 nm wide Cu lines : Impact of different interfaces on failure mode," *IEEE*, 2013.

[4] H. Shimizu, Y. Suzuki, T. Nogami, N. Tajima, T. Momose, Y. Kobayashi, and Y. Shimogaki, "CVD and ALD Co(W) Films Using Amidinato Precursors as a Single-Layered Barrier/Liner for Next-Generation Cu-Interconnects," *ECS J. Solid State Sci. Technol.*, vol. 2, no. 7, pp. P311–P315, May 2013.

[5] J. Wu, J. Li, C. Zhou, X. Lei, T. Gaffney, J. a. T. Norman, Z. Li, R. Gordon, and H. Cheng, "Computational Study on the Relative Reactivities of Cobalt and Nickel Amidinates via β-H Migration," *Organometallics*, vol. 26, no. 11, pp. 2803–2805, May 2007.

[6] H. B. Bhandari, J. Yang, H. Kim, Y. Lin, R. G. Gordon, Q. M. Wang, J.-S. M. Lehn, H. Li, and D. Shenai, "Chemical Vapor Deposition of Cobalt Nitride and its Application as an Adhesion-Enhancing Layer for Advanced Copper Interconnects," *ECS J. Solid State Sci. Technol.*, vol. 1, no. 5, pp. N79–N84, Sep. 2012.

[7] Z. Li, D. K. Lee, M. Coulter, L. N. J. Rodriguez, and R. G. Gordon, "Synthesis and characterization of volatile liquid cobalt amidinates.," *Dalton Trans.*, no. 19, pp. 2592–2597, May 2008.

[8] H.-B.-R. Lee, W.-H. Kim, J. W. Lee, J.-M. Kim, K. Heo, I. C. Hwang, Y. Park, S. Hong, and H. Kim, "High Quality Area-Selective Atomic Layer Deposition Co Using Ammonia Gas as a Reactant," *J. Electrochem. Soc.*, vol. 157, no. 1, pp. D10–D15, 2010.

[9] T. D. Elko-hansen, A. D. Dolocan, and J. G. Ekerdt, "Interdiffusion and diffusive stabilization of cobalt by copper during atomic layer deposition from bis (N- tert-butyl- N ' -ethylpropionamidinato) cobalt (II)," *Rev.*, pp. 1–13, 2014.

[10] L. T. Zhuravlev, "The surface chemistry of amorphous silica. Zhuravlev model," *Colloids Surfaces A Physicochem. Eng. Asp.*, vol. 173, no. 1–3, pp. 1–38, Nov. 2000.

[11] H. Lee and S. F. Bent, "Nanopatterning by Area-Selective Atomic Layer Deposition," in in *Atomic Layer Deposition of Nanostructured Materials*, N.

(University of A. Pinna and M. Knez, Eds. Weinheim: Wiley-VCH Verlag & Co. KGaA, 2012, pp. 193–225.

[12] S. F. Bent, J. S. Kachian, J. C. F. Rodríguez-Reyes, and A. V Teplyakov, "Tuning the reactivity of semiconductor surfaces by functionalization with amines of different basicity.," *Proc. Natl. Acad. Sci. U. S. A.*, vol. 108, no. 3, pp. 956–60, Jan. 2011.

[13] L. L. Crowe and L. M. Tolbert, "Silica passivation efficiency monitored by a surface-bound fluorescent dye.," *Langmuir*, vol. 24, no. 16, pp. 8541–6, Aug. 2008.

[14] K. L. Chavez and D. W. Hess, "A Novel Method of Etching Copper Oxide Using Acetic Acid," *J. Electrochem. Soc.*, vol. 148, no. 11, pp. G640–G643, 2001.

[15] B. D. Hatton, K. Landskron, W. J. Hunks, M. R. Bennett, D. Shukaris, D. D. Perovic, and G. A, "Materials chemistry for low-k materials," *Mater. Today*, vol. 9, no. 3, pp. 22–31, 2006.

Chapter 4: Summary

4.1 CONCLUSIONS

The interactions of CoAMD on Cu, SiO_2 and CDO were investigated to support the development of area-selective atomic layer deposition (AS-ALD) of Co capping layers on Cu interconnects. Adsorption studies demonstrated that Co from CoAMD accumulates preferentially on Cu metal substrates via a complex dissociative chemisorption mechanism. Accumulation of Co on Cu from CoAMD is ALD-like and self-limited by the slow desorption of amidinate ligands and fragments from the Cu surface. Co deposition by ALD from CoAMD proceeds first by a metastable 2D Co-rich layer that grows on the Cu substrate until enough Co is deposited that the film begins to roughen and grow three dimensionally. The Co-rich layer remains while Co continues to accumulate as indicated by ToF-SIMS depth profiling. Further, a surfactant-like Cu layer is apparent on the surface of the Co up to at least 16 nm film thicknesses suggesting that the lower energy Cu plays a role in the Co deposition and may stabilize the Co film especially at the early stages of film deposition by surface segregating to reduce the free surface energy. The Cu surface layer may improve Co lattice matching as pseudoepitaxial fcc and hcp Co grains can be expected on the Cu surface. X-ray diffraction studies revealed strong fcc (111) signals for blank Cu wafers and 4.5 nm Co/Cu film samples. However, distinct hcp signals were indiscernible from the signal noise and the Co contribution to the fcc signal is inseparable from the Cu contribution due to the magnitude of the signal. Finally, highly mobile Cu and Co at the film interface leads to significant intermixing of the species during Co deposition even at 265 °C as well as grain boundary diffusion of Cu through the Co film. It should be mentioned that, as with most CVD and ALD process, finite C and N contaminants were incorporated in the Co films especially at lower temperature depositions. While the majority of the amidinate fragments are removed during the inert gas sweep and the second

half-cycle, some amidinate fragments are incorporated into the subsequent Co film as C and N impurities. CoAMD interactions with SiO_2 and CDO surfaces appear strongest with exposed OH moieties as indicated by the faster initial accumulation of CoAMD on SiO_2 than on CDO during adsorption experiments. CoAMD may also deposit on strained siloxane surface species but to a lesser extent given the lower reactivity of strained siloxane bridges relative to OH moieties. Both SiO_2 and CDO favored the formation of oxidized Co^{2+} and possibly Co^{3+} species and some partially reacted CoAMD precursor. The shakeup signals in the Co 2*p* X-ray photoelectron spectra are a strong indication of paramagnetic Co^{2+}. The inherent preference of CoAMD to deposit on transition metals like Cu versus dielectric surfaces bodes well for applications in selective ALD. Because CoAMD readily deposits at existing, unoccupied Co surface sites, it is critical to fully passivate the dielectric surfaces to eliminate Co accumulation on CDO during film growth. Enhanced surface selectivity for Co capping layers can be achieved using CoAMD and by leveraging low-temperature ALD with dielectric-surface chemical passivation. By reducing the deposition temperature from 265 °C to 165 °C the preference for Co accumulation on Cu versus CDO improved from 2.5:1 to 5:1 by atomic percent. Extended trimethylchlorosilane (TMCS) exposures were the most effective to produce surface selectivity for Co deposition on Cu rather than on CDO. For a 50 cycle deposition at 165 °C, Co accumulated selectively on Cu 30:1 versus CDO after a 500 kTorr-s TMCS at 50 °C.

4.2 Recommendations for Future Work

Previous efforts have demonstrated that amorphous metal caps resist cross-barrier diffusion better than polycrystalline films. Electroless and CVD or ALD deposited CoWP is amorphous depending primarily on the concentration of P. W may also serve to fill grain boundaries of the polygranular Co films decreasing susceptibility to grain-boundary diffusion. The selectivity-enhanced deposition of Co from CoAMD presented in this

research would benefit from investigations that incorporate ALD with a W amidinate like bis(tert-butylimino)bis(dimethylamino) tungsten (W-AMD). CVD and ALD of Co(W) has been demonstrated using CoAMD and W-AMD with NH_3 at 350-400 °C by Shimizu, *et al.* [1,2]. Further, Henderson *et al.* demonstrated that amorphous Co(P) films could be prepared under CVD conditions using trimethylphosphine (TMP) as the P source [3]. To extend these systems for applications in selectivity, it would be important to evaluate whether low-temperature ALD processes are feasible for the incorporation of P from TMP or W from W-AMD while maintaining the selectivity of the CoAMD process. Because the deposition of amidinates on transition metals proceeds by similar mechanisms, it is possible that the W-AMD process could be made selective by the same passivation treatments explored for CoAMD. Further, it would be important to understand how the TMP affects the surface reactivity of the CDO surface and, especially, whether the TMP exposure would generate new reactive surface species after passivation that might lead to unwanted Co accumulation.

Further, the use of reversible adsorbates like CO has been demonstrated to improve thin film growth by encouraging more uniform nucleate formation on hydroxylated surfaces [4]. The reversible physisorption of CO might also be used as a passivant by maintaining a suitable overpressure of CO throughout the ALD of Co films by blocking free-hydroxyl sites at the surface. Moreover, if the dielectric surface passivation was incomplete after an exposure to, *e.g.,* TMCS, CO might be used to augment the passivation and further improve the selectivity of CoAMD for the Cu surface versus CDO. One caveat to this proposal is that CO was also shown to block Ru deposition at exisiting Ru nucleates, leading to more uniform nucleation across the oxide surface. For the Co system, even if CO inhibited some accumulation at the Co or Cu surface, as long as the relative nucleation

rates strongly favored CoAMD deposition on Cu versus CDO, the improvement of selectivity would be a success.

Finally, metals deposition from amidinate precursors has been performed using NH_3 rather than H_2 or with a mixture of the two gases. In these cases, the deposition rates are generally reported as being higher with NH_3 than with H_2 although some H_2 is generally necessary for film densification and clearing of amidinate ligands and fragments [5–7]. Applying NH_3 to the selective ALD methods presented herein might increase the Co film deposition rate on Cu. It would be important to evaluate whether NH_3 is amenable to the chemical passivation schemes and, if amorphous Co(P) films are targeted, whether this is possible without H_2 introduction.

4.6 References

[1] H. Shimizu, A. Kumamoto, K. Shima, and Y. Kobayashi, "Self-Assembled Nano-Stuffing Structure in CVD and ALD Co (W) Films as a Single-Layered Barrier / Liner for Future," vol. 2, no. 11, pp. 471–477, 2013.

[2] H. Shimizu, A. Kumamoto, and K. Shima, "Process design for Co (W) alloy films as a single layered barrier / liner layer for 14nm generation Cu - interconnect Why CVD / ALD - Co (W) films ? Why CVD / ALD - Co (W) films ? Co (W) films using carbonyl precursors Cobalt deposition using meta," pp. 1–6, 2012.

[3] L. B. Henderson and J. G. Ekerdt, "Effect of Phosphorus and Carbon Incorporation in Amorphous Cobalt Films Prepared by Chemical Vapor Deposition," *J. Electrochem. Soc.*, vol. 157, no. 1, p. D29, 2010.

[4] W. Liao and J. G. Ekerdt, "Effect of CO on Ru Nucleation and Ultra-Smooth Thin Film Growth by Chemical Vapor Deposition at Low Temperature," *Chem. Mater.*, vol. 25, pp. 1793–1799, 2013.

[5] H. B. Bhandari, J. Yang, H. Kim, Y. Lin, R. G. Gordon, Q. M. Wang, J.-S. M. Lehn, H. Li, and D. Shenai, "Chemical Vapor Deposition of Cobalt Nitride and its Application as an Adhesion-Enhancing Layer for Advanced Copper Interconnects," *ECS J. Solid State Sci. Technol.*, vol. 1, no. 5, pp. N79–N84, Sep. 2012.

[6] R. G. Gordon, H. Kim, and H. Bhandari, "Cobalt Nitride Layers for Copper Interconnects and Methods for Forming Them," US 2008/0254232 A12008.

[7] H. Li, D. B. Farmer, R. G. Gordon, Y. Lin, and J. Vlassak, "Vapor Deposition of Ruthenium from an Amidinate Precursor," *J. Electrochem. Soc.*, vol. 154, no. 12, pp. D642–D647, 2007.

SECTION 2: HETEROATOM ENHANCEMENT OF HOPG FOR ENHANCED PARTICLE NUCLEATION AND STABILIZATION

Chapter 5: Enhanced Nucleation of Pt Particles on Boron-Treated Highly Oriented Pyrolytic Graphite via Chemical Vapor Deposition

5.1 INTRODUCTION

In the interest of extending the lifetime of available fossil-based energy resources, the development of alternative energies and energy devices is paramount. Fuel cells offer one such alternative. In particular, direct methanol fuel cells (DMFCs) offer a unique alternative to internal combustion engines and gasoline or diesel generators. Fuel cells are particularly appealing because of their higher operating efficiency and low pollutant production [1,2]. Nevertheless, DMFCs are still subject to technological and eco- nomic challenges. Specifically, there is impetus to reduce the cost and increase the performance of DMFC anodes by designing catalyst alloys that efficiently dissociate methanol into hydrogen and carbon substituents and by optimizing catalyst dispersion and size distribution [3-6]. DMFC anode catalysts are generally Pt or Pt/Ru alloys on carbon black or highly oriented pyrolytic graphite (HOPG) supports [5,6]. This study focuses on improving metal dispersion on and adhesion to HOPG.

Generally, HOPG is a poor wetting surface for metals [7,8]. Consequently, metal adatoms tend to adhere to defects on the graphite surface. Aktary et al. described the nucleation of Pt on HOPG as a nanobead structure along grain-boundary defects at low coverage that catalyze adatom adsorption on the basal plane at higher Pt coverage [9]. To reduce the cost of DMFC anodes, however, it is necessary to limit the Pt coverage while maximizing catalytic surface area. Through careful control of synthesis variables, defect-mediated growth is an effective means to control Pt particle size and distribution [10-13].

Defect-mediated growth is a well-researched method of trap site-controlled nucleation and has been widely applied to transition metal growth on carbon substrates [8-17]. Defects are generated on HOPG by physical and chemical methods. Physical methods include ion-beam implantation, etching, and sputtering [7,8,17-21]. Chemical methods such as surface oxidation and heteroatom doping have also been demonstrated to generate traps on HOPG [14-16,19]. B and N dopants are common choices for HOPG because of their similar size to C and their ability to incorporate readily into sp^2-hybridized C [3,14-16]. Electron energy loss spectroscopy studies have investigated the sp^2 nature of HOPG and demonstrated boron's solubility in HOPG and its incorporation with sp^2-hybridized graphite structures [22-24]. It has been further demonstrated that B dopant atom p-orbitals interact favorably with Pt d-orbitals to provide trap sites for particle nucleation [3,15,16].

Previously, Zhou et al. and Acharya et al. used first principles calculations to demonstrate that Pt particles can be stabilized on HOPG by chemically modifying the HOPG surface with boron and nitrogen [14,16]. This work expands on their efforts by exposing HOPG to B using hot-wire chemical vapor deposition (HWCVD) and observing Pt nucleation behavior on the resulting surface. B-treatment is achieved by cracking B_2D_6 with a hot- wire filament near the HOPG surface.

5.2 Experimental Methods

ZYA grade HOPG substrates (10 mm × 10 mm × 1.5 mm) were obtained from NT-MDT Co. The substrates were treated by one of three methods before Pt deposition. While all three methods include a previously described mechanical cleaving process [25,26], AHOPG and BHOPG samples underwent further treatment before synthesis. AHOPG and BHOPG samples were treated in a separate apparatus that comprises a furnace, analytical chamber, and HWCVD chamber connected through a transfer chamber. The details of the HWCVD apparatus have been previously described [27,28]. AHOPG samples were

annealed for 15min at 700-720 °C before deposition. BHOPG samples were annealed in the same manner as AHOPG samples but subsequently dosed with diborane (B_2D_6) (1% B_2D_6 in He, Voltaix). Except for the correlation tests between B-exposure and Pt surface density, BHOPG samples were exposed to 6.0 L (6.0×10^{-6} Torr × s) B_2D_6, that led to 7 × 10^{14} B/cm2. P_{total} was 2.0×10^{-6} Torr for HWCVD including the He carrier gas. Treated AHOPG and BHOPG samples were transferred *ex situ* from the HWCVD apparatus to the deposition chamber (described below) for Pt deposition. The prepared substrates were attached to 1 in. diameter stainless steel pucks using Ta foil (Aesar, 99.95%) and mounted in the Pt deposition apparatus. The deposition apparatus comprises a cold-wall CVD chamber with multiple saturator-based precursor inlets and an analytical chamber housing a PHI (Physical Electronics) model 1600 X-ray photoelectron spectroscopy (XPS) system [29]. The chambers are connected via an in situ transfer tube, and samples are introduced to the chamber through a central load lock. Turbomolecular pumps on the analytical chamber and transfer tube maintain low pressure. The CVD chamber vacuum is controlled separately by a roughing pump or a diffusion pump depending on the operation. Samples in the CVD chamber underwent backside heating from an infrared bulb, and sample temperatures were approximated using a thermocouple attached to a fused silica wafer on an equivalent steel puck [29]. Sample temperatures are considered accurate to within 10 °C. In the CVD chamber, the substrate was heated to 193 °C under pressure-controlled flow of H2 at 0.340-0.375 Torr. To approach thermal equilibrium under these conditions, the substrate was allowed to heat for a minimum of 2h. The trimethyl-(methylcyclopentadienyl)platinum(IV) ($CH_3CpPt(CH_3)_3$, Strem Chemicals, 99%) precursor was heated to 38 °C. Although many Pt CVD precursors are available, $CH_3CpPt(CH_3)_3$ was chosen for its relative volatility, for simple handling (liquid at room temperature), and for the relatively carbon-free films produced using this precursor [30-

32]. Once thermal equilibrium was achieved, the chamber was evacuated to between 0.020 and 0.030 Torr and the chamber was sealed from vacuum. During Pt synthesis, H_2 flows at a rate of 3.0 sccm through a saturator tube of the preheated $CH_3CpPt(CH_3)_3$.The precursor-carrying stream flows into the CVD chamber perpendicularly to the substrate. The chamber was allowed to pressurize under precursor flow for 5 min and reached a maximum pressure of 0.330-0.340 Torr for 5-min syntheses. Pt growth was controlled by substrate temperature and synthesis time, and the maximum pressure was a consequence of the carrier gas flow rate and the size of the synthesis chamber. Pressure-synthesis correlations were not investigated in this work. After 5 min, precursor flow and substrate heating were terminated and the chamber was evacuated. The platinized substrate was allowed to cool to <75 °C and transferred *in situ* to the analysis chamber. After XPS analysis, the samples were transferred in air to a Zeiss Supra 40 VP scanning electron microscope for SEM imaging. Thirty min depositions were performed in the same manner as 5 min depositions except that heating was maintained for the full thirty min while pressurization of the chamber ceased at 0.750 Torr after 10 min. Thermal stability experiments were performed in a Carbolite HST12/400 clam-shell oven. Ramp rates were controlled using built-in PID controls and monitored with a separate *in situ* thermocouple. Samples were heated under Ar flow (99.999%, Matheson) of 10-20 sccm. During stability tests, samples were heated to 250 °C at 20 °C/min and 5 °C/min to their final temperature. Heating ceased when the oven stabilized at the desired temperature. The sample surface was imaged after each sub-sequent anneal for variations in average Pt particle size.

5.3 Results

XP spectra verified Pt content and C signatures. XPS sensitivity was insufficient to detect B species for 6 L B_2D_6 dosed BHOPG; however, B presence is demonstrated in HOPG for a larger, 12 L B_2D_6 dose (Figure 5.1). Li et al. proposed that B atoms are

incorporated into the sp^2 C structure of carbon nanotubes and form pyridine-like structures to which the Pt adatoms adhere [3]. Figure 5.2 depicts possible B-C structures. While a larger variety of B-B-C and B-C structures are possible at higher B concentrations, these B-αC and B-C pyridine-like structures proposed by Li et al. and Acharya et al. are possible candidates for our BHOPG surfaces [3,15,16]. For such structures, the binding energy of Pt on B-doped graphite is proposed to increase by as much as 100% compared with pristine graphite (-9.41 kcal/mol, $C_{70}H_{22}$; -18.76 kcal/mol, $C_{66}H_{12}B$) [16]. Acharya et al. demonstrated with a first-principles graphene model that Pt_6 adsorbed on $C_{42}B_8$ with an energy of -19.2 kcal/mol versus -2.3 kcal/mol on C50 [15].

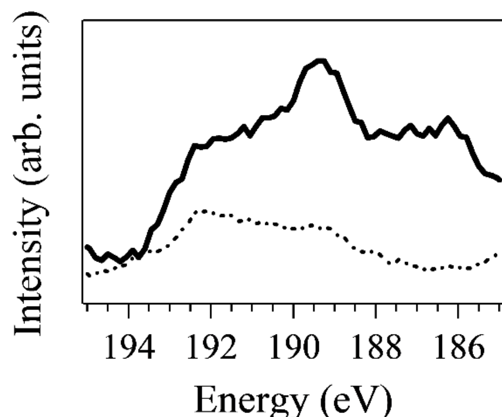

Figure 5.1. XP spectra of B 1s signal (BE 189.4 eV) in HOPG that underwent 12 L B2D6 exposure (——) and no exposure (• • • •)

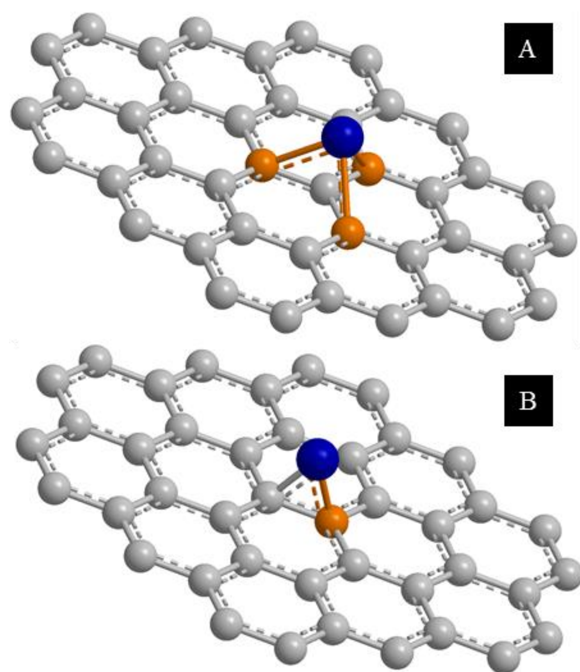

Figure 5.2. Possible structures for B enhanced Pt binding sites where Pt atoms are blue, B atoms orange, and C grey. A) represents pyridine-like bond structure and B) represents Pt bridging from B to α-C.

SEM images illustrate Pt growth patterns on HOPG, AHOPG, and BHOPG substrates (Figures 5.3 and 5.4). Results indicate that BHOPG substrates provided more disperse sites for Pt adatom nucleation. At low Pt coverage, BHOPG samples exhibit nearly monodisperse Pt particles, 5 ± 1.5 nm diameter, whereas HOPG and AHOPG substrates exhibit preferential growth along grain boundary defects and at isolated kink and island defects in the basal plane. Though we observed nucleation along grain boundaries for all samples, Figures 5.3 and 5.4 demonstrate that Pt particle nucleation in the basal plane is greatest for BHOPG samples (rightmost image in Figures 5.3 and 5.4). HOPG substrates (leftmost in Figures 5.3 and 5.4) exhibited some additional basal plane growth at kink and ledge defects most likely generated by uneven cleaving and the

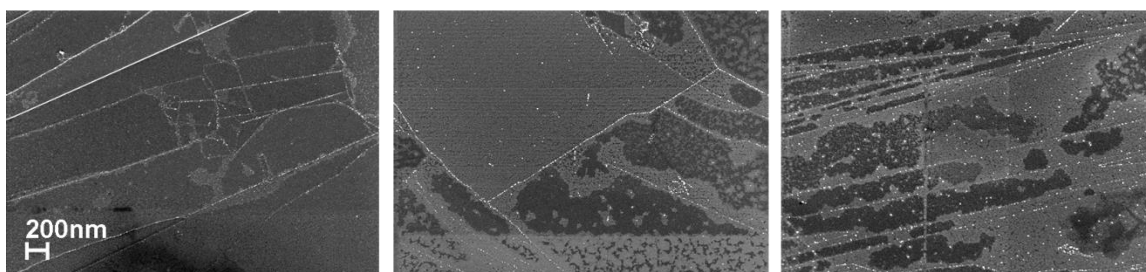

Figure 5.3. SEM of Pt coverage after 5 min Pt synthesis. Left to Right: Pt on HOPG, Pt on AHOPG, Pt on BHOPG.

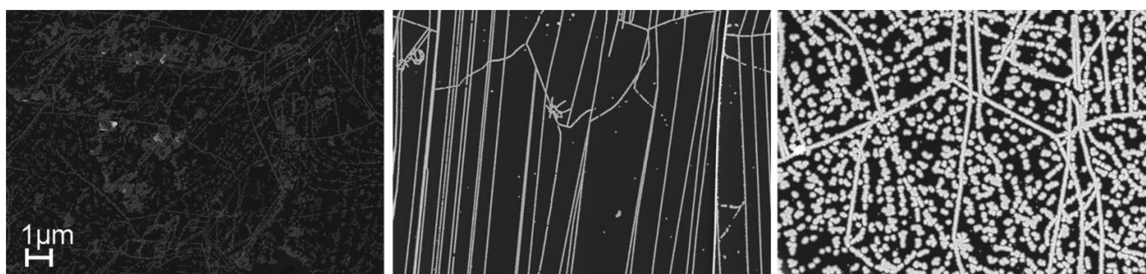

Figure 5.4. SEM of Pt coverage after 30 min Pt synthesis. Left to Right: Pt on HOPG, Pt on AHOPG, Pt on BHOPG.

nanobead catalyzing effect proposed by Aktary et al. [9]. Nanobead growth is evidenced by 30 min growth times for Pt on HOPG as depicted in Figure 5.4. This pattern is not observed for 5 min growths and minimally for BHOPG samples even at longer growth times. BHOPG samples exhibit essentially conformal growth at grain boundary defects and in the basal plane as evidenced by conformal Pt particle size across BHOPG substrates (rightmost image of Figures 5.3 and 5.4). In contrast, longer growths resulted in smaller Pt particles in the basal plane than at grain defects for HOPG and AHOPG substrates, in agreement with the nanobead effect [9]. AHOPG samples (middle image of Figures 5.3 and 5.4) consistently showed little or no nucleation in the basal plane. Ledge and kink defects in the basal plane were likely ameliorated by the high

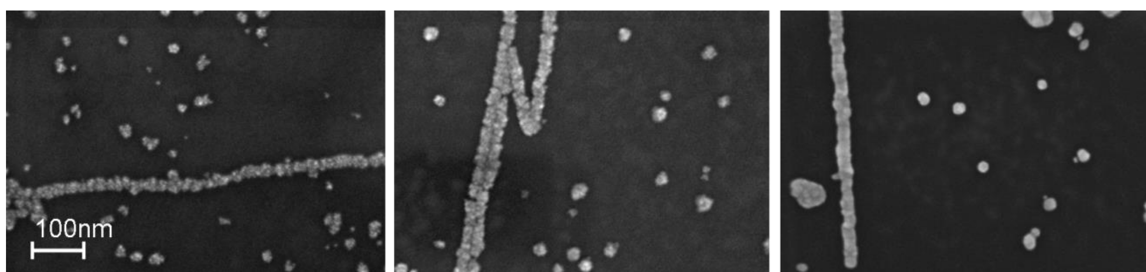

Figure 5.5. SEM images from thermal stability study – 30 min Pt deposition on BHOPG. Left to Right: unmodified Pt on BHOPG, annealed to 300 °C, annealed to 500 °C.

temperature annealing step for AHOPG and BHOPG samples. We infer that traps in the BHOPG basal plane are from B dosing and not from cleaving in the majority of the samples because kink and ledge defects are readily identified in SEM.

It is noteworthy that large variations in nucleation were also observed for substrates from different stock and, less frequently, after successive cleavings of a single substrate. On several occasions, particle density increased by orders of magnitude after cleaving with no change to the experimental method. Such outliers were discarded from this study. All grouped images are from the same stock of HOPG.

Thermal stability studies were performed on 30 min deposition samples to evaluate the adhesion of Pt particles to BHOPG substrates qualitatively (Figure 5.5). On average, particle agglomeration was not observed on samples annealed up to 500 °C. The average particle size was 15-20 nm for as-grown samples and samples annealed up to 500 °C. As the SEM images do not depict the same surface location and the Zeiss SEM did not have an in situ stage heater, the diffusion of Pt particles under higher temperature could not be followed and requires further research. The thermal stability of these Pt particles is not necessarily indicative of Pt resistance to electromigration for which further investigation is necessary.

Figure 5.6 illustrates that Pt particle density increases with increasing B_2D_6 exposure. For 5 min Pt deposition, particles had an average size of 5 ± 1.5 nm.

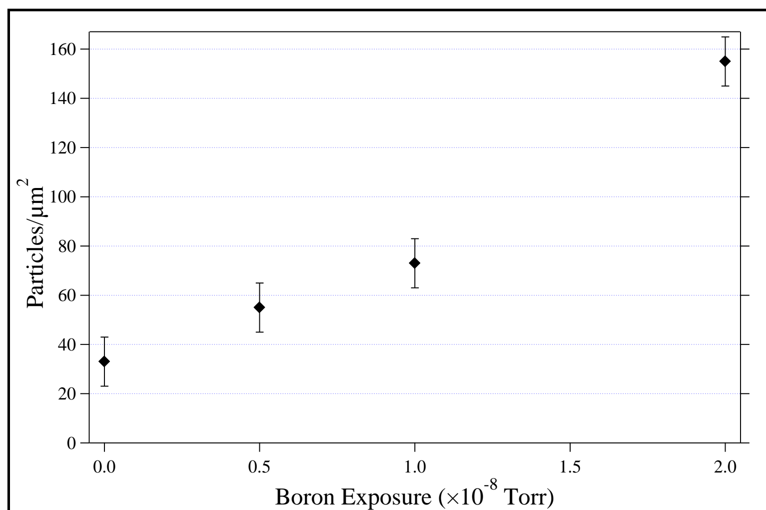

Figure 5.6. Particle density vs. boron exposure.

5.4 Discussion

While ion-beam implantation and sputtering are effective methods of generating defects in the HOPG basal plane, chemical methods have also shown promise and scale more easily than electron gun-based processes. Endo et al. demonstrated that annealing HOPG in the presence of B_4C powder chemically generates trap sites on the HOPG surface [33]. In contrast to the B_4C powder method, we cracked B_2D_6 gas using a hot-wire filament near the substrate surface. Due to low B sensitivity in XPS, an extended, 12 L B_2D_6 exposure was employed to demonstrate that B is delivered to the surface during HWCVD (Figure 5.1). Since there is no induction time in cracking B_2D_6, we infer that B is also present for the 6 L exposure used to prepare the BHOPG substrates. The B remaining on the HOPG surface after annealing is likely bonded to the sp^2 carbon matrix of the HOPG. For XP spectra, the B 1s signature appears as a 189 eV peak. A broader B signature is apparent from 186 to 192 eV due to B_xC_y and $B_xC_yO_z$ species present on the substrate that

have been previously identified [34-36]. Sample oxidation is a result of multiple ex situ transfers during the detection of B. However, after a single transfer from the HWCVD to the synthesis chamber, the BHOPG XP spectra exhibited no O peak. Consequently, it is believed that BHOPG samples were negligibly oxidized prior to Pt deposition. Moreover, since all samples underwent the same air exposure before synthesis, it is reasonable to assume that oxide defects are negligible influences on nucleation as compared with B contributions. Further investigation is necessary to completely characterize the effect of B oxide species on Pt nucleation and dispersion. Nucleation density on the HOPG basal plane increased proportionally with increasing B_2D_6 exposure (Figure 5.6). That HOPG and AHOPG also exhibited nucleation in the basal plane is an indication of cleavage-generated defects and defects inherent on the basal-plane surface. However, the considerably higher Pt particle density on BHOPG substrates and the proportionality of Pt particle density to B_2D_6 exposure validate the stabilizing interaction between the B p-orbital and Pt d-orbital as indicated by Li et al. and Acharya et al. [3,15,16].

The growth density and size of the deposited Pt nanoparticles can be controlled by manipulating the boron exposure and Pt synthesis time. Moreover, boron-treated Pt substrates exhibited Pt particle densities considerably higher than those for comparable HOPG and AHOPG substrates even at nominal 6 L B_2D_6 exposures (Figures 5.3, 5.4, and 5.6).

Nevertheless, B-doping occurs without preference across the HOPG surface. This means that intrinsic trap sites such as grain boundaries and cleavage-generated defects will also be exposed to BDx fragments. For instance, nanobead growth patterns reported by Aktary et al. were observed in HOPG, in AHOPG, and, to a lesser degree, in BHOPG samples particularly for longer growths as Pt particles grew beyond 10-20 nm in diameter [9]. The optimization of the Pt particle dispersion and size is, therefore, limited to the

HOPG basal planes for higher Pt content since nanobead growth patterns are exhibited along grain boundaries for all HOPG substrates, whether boron-treated or not.

This study demonstrates that Pt particle nucleation on HOPG may be optimized using dopants such as B to promote scalable, defect-mediated growth. The defects likely comprise pyridine-like B-C and B-αC species that trap Pt adatoms as they diffuse across the HOPG surface [3,15,16]. As adatoms generally agglomerate at surface defects, nucleation is also observed at cleavage- generated defects [10,26,37].

5.5 REFERENCES

[1] EG&G Technical Services Inc. Fuel Cell Handbook, 7th ed.; U.S. Department of Energy: Morgantown, WV, 2004.

[2] Service, R. F. Science 2002, 296, 64–66.

[3] Li, Y.-H.; Hung, T.-H.; Chen, C.-W. Carbon 2009, 47, 850–855.

[4] Park, G.-G.; Yang, T.-H.; Yoon, Y.-G.; Lee, W.-Y.; Kim, C.-S. Int. J. Hydrogen Energy 2003, 28, 645–650.

[5] Lee, Y. H.; Lee, G.; Shim, J. H.; Hwang, S.; Kwak, J.; Lee, K.; Song, H.; Park, J. T. Chem. Mater. 2006, 18, 4209–4211.

[6] Petrii, O. A. J. Solid State Electrochem. 2008, 12, 609–642.

[7] Yang, D.-Q.; Sacher, E. Surf. Sci. 2002, 516, 43–55.

[8] Yang, D.-Q.; Sacher, E. J. Phys. Chem. C 2008, 112, 4075–4082.

[9] Aktary, M.; Lee, C. E.; Xing, Y.; Bergens, S. H.; McDermott, M. T. Langmuir 2000, 16, 5837–5840.

[10] Ratsch,C.;Venables, J. A. J. Vac. Sci. Tech. A 2003, 21, S96–S109.

[11] Wedding, J. B.; Wang, G.; Lu, T.-M. Surf. Sci. 2002, 504, 28–36.

[12] Giulian, R.; Kluth, P.; Araujo, L. L.; Llewellyn, D. J.; Ridgway, M. C. Appl. Phys. Lett. 2007, 91 (093115), 1–3.

[13] Venables, J. A.; Giordano, L.; Harding, J. H. J. Phys.: Condens. Matter 2006, 18, S411–S427.

[14] Zhou,Y.;Pasquarelli,R.;Holme,T.;Berry, J.;Ginley,D.;O'Hayre, R. J. Mater. Chem. 2009, 19, 7830.

[15] Acharya, C. K.; Sullivan, D. I.; Turner, C. H. J. Phys. Chem. C 2008, 112, 13607–13622.

[16] Acharya, C. K.; Turner, C. H. J. Phys. Chem. B 2006, 110, 17706–17710.

[17] Zhu, Y.-J.; Schnieders, A.; Alexander, J. D.; Beebe, T. P., Jr. Langmuir 2002, 18, 5728–5733.

[18] Nicholson, K. T.; Minton, T. K.; Sibener, S. J. J. Phys. Chem. B 2005, 109, 8476–8480.

[19] Bock, C.; MacDougall, B.; Chang, S.; Botton, G.; Kingston, D.; Halvorsen, H. Electrochem. Soc. 2008, 216.

[20] Collart, E. J. H.; Weemer, K.; Gravesteijn, D. J.; van Berkum, J. G. M. J. Vac. Sci. Technol. B 1998, 16, 280.

[21] Ritter, R.; Kowarik, G.; Meissl, W.; S€uss, L.; Maunoury, L.; Lebius, H.; Dufour, C.; Toulemonde, M.; Aumayr, F. Nuclear Instrum. Methods Phys. Res., Sect. B 2010, 268, 2897–2900.

[22] Serin, V.; Brydson, R.; Scott, A.; Kihn, Y.; Abidate, O.; Maquin, B.; Derre, A. Carbon. 2000, 38, 547–554.

[23] Papworth, A. J.; Kiely, C. J.; Burden, A. P.; Silva, S. R. P.; Amaratunga, G. A. J. Phys. Rev. B 2000, 62, 12628–12631.

[24] Papageorgiou, N.; Portail, M.; Layet, J. M. Surf. Sci. 2000, 454-456, 462–466.

[25] Prodanov, N. V.; Khomenko, A. V. Surf. Sci. 2010, 604, 730–740.

[26] Liu, Z.; Zheng, Q.-S.; Liu, J.Z. Appl.Phys. Lett. 2010, 96, 201909(1-3).

References

A. Ceyhan and A. Naeemi, “Cu / Low- k Interconnect Technology Design and Benchmarking for Future Technology Nodes,” IEEE Trans. Electron Devices, vol. 60, no. 12, pp. 4041–4047, 2013.

A. Christensen, A. V Ruban, P. Stoltze, K. W. Jacobsen, H. L. Skriver, J. K. No, and F. Besenbacher, “Phase diagrams for surface alloys,” vol. 56, no. 10, pp. 5822–5834, 1997.

A. Kohn, M. Eizenberg, and Y. Shacham-Diamand, “Copper grain boundary diffusion in electroless deposited cobalt based films and its influence on diffusion barrier integrity for copper metallization,” J. Appl. Phys., vol. 94, no. 5, p. 3015, 2003.

Acharya, C. K.; Sullivan, D. I.; Turner, C. H. J. Phys. Chem. C 2008, 112, 13607–13622.

Acharya, C. K.; Turner, C. H. J. Phys. Chem. B 2006, 110, 17706–17710.

Aktary, M.; Lee, C. E.; Xing, Y.; Bergens, S. H.; McDermott, M. T. Langmuir 2000, 16, 5837–5840.

Arnaud, L.; Cacho, F.; Doyen, L.; Terrier, F.; Galpin, D.; Monget, C. Microelectron. Eng. 2010, 87, 355–360.

Arnaud, L.; Tartavel, G.; Berger, T.; Mariolle, D.; Gobil, Y.; Touet, I. In 37th Annual International Reliability Physics Symposium; San Diego, CA, 1999; pp. 263–269.

Aubel, O.; Hennesthal, C.; Hauschildt, M.; Beyer, A.; Poppe, J.; Talut, G.; Gall, M.; Hahn, J.; Boemmels, J.; Nopper, M.; Seidel, R. IEEE 2011, 26–28.

B. D. Hatton, K. Landskron, W. J. Hunks, M. R. Bennett, D. Shukaris, D. D. Perovic, and G. A, “Materials chemistry for low-k materials,” Mater. Today, vol. 9, no. 3, pp. 22–31, 2006.

B. P. Tonner, Z.-L. Han, and J. Zhang, “Structure of Co films grown on Cu(111) studied by photoelectron diffraction,” Phys. Rev. B, vol. 47, no. 15, pp. 9723–9732, 1993.

B. S. Lim, A. Rahtu, and R. G. Gordon, “Atomic layer deposition of transition metals.,” Nat. Mater., vol. 2, no. 11, pp. 749–754, Nov. 2003.

Bahlawane, N.; Kohse-Höinghaus, K.; Premkumar, P. A.; Lenoble, D. Chem. Sci. 2012, 3, 929–941.

Bock, C.; MacDougall, B.; Chang, S.; Botton, G.; Kingston, D.; Halvorsen, H. Electrochem. Soc. 2008, 216.

C. Chou and W. Dow, “Formation of CoWP Barrier Layer by Electroless Deposition for TSV Metallization,” p. 2010.

C. S. Hau-Riege and C. V. Thompson, “Electromigration in Cu interconnects with very different grain structures,” Appl. Phys. Lett., vol. 78, no. 22, pp. 3451–3453, 2001.

C. S. Hau-Riege, “An introduction to Cu electromigration,” Microelectron. Reliab., vol. 44, no. 2, pp. 195–205, Feb. 2004.

C.-C. Yang, P. Flaitz, P.-C. Wang, F. Chen, and D. Edelstein, “Characterization of Selectively Deposited Cobalt Capping Layers: Selectivity and Electromigration Resistance,” IEEE Electron Device Lett., vol. 31, no. 7, pp. 728–730, Jul. 2010.

C.-K. Hu, L. Gignac, R. Rosenberg, E. Liniger, J. Rubino, C. Sambucetti, A. Domenicucci, X. Chen, and a. K. Stamper, “Reduced electromigration of Cu wires by surface coating,” Appl. Phys. Lett., vol. 81, no. 10, pp. 1782–1784, 2002.

C.-K. Hu, L. Gignac, S. G. Malhotra, R. Rosenberg, and S. Boettcher, “Mechanisms for very long electromigration lifetime in dual-damascene Cu interconnections,” Appl. Phys. Lett., vol. 78, no. 7, pp. 904–906, 2001.

Chavez, K. L.; Hess, D. W. J. Electrochem. Soc. 2001, 148, G640-G643.

Collart, E. J. H.; Weemer, K.; Gravesteijn, D. J.; van Berkum, J. G. M. J. Vac. Sci. Technol. B 1998, 16, 280.

Dai, M.; Kwon, J.; Halls, M. D.; Gordon, R. G.; Chabal, Y. J. Langmuir 2010, 26, 3911–39177.

Ding, P. J.; Lanford, W. A.; Hymes, S.; Murarka, S. P. Appl. Phys. Lett. 1994, 64, 2897–2899.

EG&G Technical Services Inc. Fuel Cell Handbook, 7th ed.; U.S. Department of Energy: Morgantown, WV, 2004.

F. J. Lamelas, C. H. Lee, H. He, W. Vavra, and R. Clarke, “Coherent fcc stacking in epitaxial Co/Cu superlattices,” Phys. Rev. B, vol. 40, no. 8, pp. 5837–5840, 1989.

Gambino, J. P. In IPFA 2010: 17th IEEE International Symposium on the Physical and Failure Analysis of Integrated Circuits; IEEE, 2010.

Giulian, R.; Kluth, P.; Araujo, L. L.; Llewellyn, D. J.; Ridgway, M. C. Appl. Phys. Lett. 2007, 91 (093115), 1–3.

Gordon, R. G.; Kim, H.; Bhandari, H. Cobalt Nitride Layers for Copper Interconnects and Methods for Forming Them. U.S. Patent 0254232 A1, 2008.

H. B. Bhandari, J. Yang, H. Kim, Y. Lin, R. G. Gordon, Q. M. Wang, J.-S. M. Lehn, H. Li, and D. Shenai, “Chemical Vapor Deposition of Cobalt Nitride and its Application as an Adhesion-Enhancing Layer for Advanced Copper Interconnects,” ECS J. Solid State Sci. Technol., vol. 1, no. 5, pp. N79–N84, Sep. 2012.

H. Lee and S. F. Bent, “Nanopatterning by Area-Selective Atomic Layer Deposition,” in in Atomic Layer Deposition of Nanostructured Materials, N. (University of A. Pinna and M. Knez, Eds. Weinheim: Wiley-VCH Verlag & Co. KGaA, 2012, pp. 193–225.

H. Li and B. P. Tonner, "Structure and growth mode of metastable fcc cobalt ultrathin films on Cu (001) as determined by angle-resolved X-ray photoemission scattering," Surf. Sci., vol. 237, pp. 141–152, 1990.

H. Li, D. B. Farmer, R. G. Gordon, Y. Lin, and J. Vlassak, "Vapor Deposition of Ruthenium from an Amidinate Precursor," J. Electrochem. Soc., vol. 154, no. 12, pp. D642–D647, 2007.

H. Shimizu, K. Sakoda, T. Momose, and Y. Shimogaki, "Atomic Layer Deposited Co(W) Film as a Single-Layered Barrier/Liner for Next-Generation Cu-Interconnects," Jpn. J. Appl. Phys., vol. 51, p. 05EB02, May 2012.

H. Shimizu, Y. Suzuki, T. Nogami, N. Tajima, T. Momose, Y. Kobayashi, and Y. Shimogaki, "CVD and ALD Co(W) Films Using Amidinato Precursors as a Single-Layered Barrier/Liner for Next-Generation Cu-Interconnects," ECS J. Solid State Sci. Technol., vol. 2, no. 7, pp. P311–P315, May 2013.

H.-B.-R. Lee, W.-H. Kim, J. W. Lee, J.-M. Kim, K. Heo, I. C. Hwang, Y. Park, S. Hong, and H. Kim, "High Quality Area-Selective Atomic Layer Deposition Co Using Ammonia Gas as a Reactant," J. Electrochem. Soc., vol. 157, no. 1, p. D10, 2010.

Hau-Riege, C. S. Microelectron. Reliab. 2004, 44, 195–205.

Hau-Riege, C. S.; Thompson, C. V. Appl. Phys. Lett. 2001, 78, 3451–3453.

Hu, C.-K.; Gignac, L.; Malhotra, S. G.; Rosenberg, R.; Boettcher, S. Appl. Phys. Lett. 2001, 78, 904–906.y

Hu, C.-K.; Gignac, L.; Rosenberg, R.; Liniger, E.; Rubino, J.; Sambucetti, C.; Domenicucci, a.; Chen, X.; Stamper, a. K. Appl. Phys. Lett. 2002, 81, 1782-1784.

International Technology Roadmap for Semiconductors - Interconnect, 2011.

Iwai, H. Microelectron. Eng. 2009, 86, 1520–1528.

J. A. Venables, Introduction to Surface and Thin Film Processes. New York, NY: Cambridge University Press, 2000.

J. D. Zimmerman, B. E. Lassiter, X. Xiao, K. Sun, A. Dolocan, R. Gearba, D. a Vanden Bout, K. J. Stevenson, P. Wickramasinghe, M. E. Thompson, and S. R. Forrest, "Control of interface order by inverse quasi-epitaxial growth of squaraine/fullerene thin film photovoltaics.," ACS Nano, vol. 7, no. 10, pp. 9268–75, Oct. 2013.

J. de la Figuera, J. E. Prieto, and R. Miranda, "Scanning-tunneling-microscopy study of the growth of cobalt on Cu(111)," Phys. Rev. B, vol. 47, no. 19, pp. 13043–13049, 1993.

J. P. Gambino, "Improved Reliability of Copper Interconnects Using Alloying," in IPFA 2010: 17th IEEE International Symposium on the Physical and Failure Analysis of Integrated Circuits, 2010.

J. Shin, “Growth and Characterization of CVD Ru and Amorphous Ru-P Alloy Films for Liner Application in Cu Interconnect.,” University of Texas at Austin, 2007.

J. Wu, J. Li, C. Zhou, X. Lei, T. Gaffney, J. a. T. Norman, Z. Li, R. Gordon, and H. Cheng, “Computational Study on the Relative Reactivities of Cobalt and Nickel Amidinates via β-H Migration,” Organometallics, vol. 26, no. 11, pp. 2803–2805, May 2007.

K. L. Chavez and D. W. Hess, “A Novel Method of Etching Copper Oxide Using Acetic Acid,” J. Electrochem. Soc., vol. 148, no. 11, pp. G640–G643, 2001.

K. M. Thom, “Growth and Characterization of Ru Films Deposited by Chemical Vapor Deposition : Towards Enhanced Nucleation and Film Properties,” University of Texas at Austin, 2009.

Kaanta, C. W.; Bombardier, S. G.; Cote, W. J.; Hill, W. R.; Kerszykowski, G.; Landis, H. S.; Poindexter, D. J.; Pollard, C. W.; Ross, G. H.; Ryan, J. G.; Wolff, S.; Cronin, J. E. 1991 Proc. Eighth Int. IEEE VLSI Multilevel Interconnect. Conf. 1991, 144–152.

Kuo, C.-L.; Lee, S.; Hwang, G. Phys. Rev. Lett. 2008, 100, 1–4.

L. B. Henderson and J. G. Ekerdt, “Chemically capping copper with cobalt,” Microelectron. Eng., vol. 87, no. 4, pp. 588–592, Apr. 2010.

L. L. Crowe and L. M. Tolbert, “Silica passivation efficiency monitored by a surface-bound fluorescent dye.,” Langmuir, vol. 24, no. 16, pp. 8541–6, Aug. 2008.

L. T. Zhuravlev, “The surface chemistry of amorphous silica. Zhuravlev model,” Colloids Surfaces A Physicochem. Eng. Asp., vol. 173, no. 1–3, pp. 1–38, Nov. 2000.

L. Vitos, A. V Ruban, H. L. Skriver, and J. Kolla, “The surface energy of metals,” Surf. Sci., vol. 411, pp. 186–202, 1998.

L. Zhang, M. Kraatz, O. Aubel, C. Hennesthal, J. Im, E. Zschech, and P. S. Ho, “Cap layer and grain size effects on electromigration reliability in Cu/low-k interconnects,” 2010 IEEE Int. Interconnect Technol. Conf., pp. 1–3, Jun. 2010.

Lee, H.-B.-R.; Kim, W.-H.; Lee, J. W.; Kim, J.-M.; Heo, K.; Hwang, I. C.; Park, Y.; Hong, S.; Kim, H. J. Electrochem. Soc. 2010, 157, D10-D15.

Lee, Y. H.; Lee, G.; Shim, J. H.; Hwang, S.; Kwak, J.; Lee, K.; Song, H.; Park, J. T. Chem. Mater. 2006, 18, 4209–4211.

Li, H.; Farmer, D. B.; Gordon, R. G.; Lin, Y.; Vlassak, J. J. Electrochem. Soc. 2007, 154, D642- D647.

Li, Y.-H.; Hung, T.-H.; Chen, C.-W. Carbon 2009, 47, 850–855.

Li, Z.; Barry, S. T.; Gordon, R. G. Inorg. Chem. 2005, 44, 1728–35.

Li, Z.; Lee, D. K.; Coulter, M.; Rodriguez, L. N. J.; Gordon, R. G. Dalton Trans. 2008, 2592–2597.

Lim, B. S.; Rahtu, A.; Gordon, R. G. Nat. Mater. 2003, 2, 749–754.

Lim, B. S.; Rahtu, A.; Park, J.-S.; Gordon, R. G. Inorg. Chem. 2003, 42, 7951–7958.

Liu, Z.; Zheng, Q.-S.; Liu, J.Z. Appl.Phys. Lett. 2010, 96, 201909(1-3).

M. F. Chioncel and P. W. Haycock, "Structural Characterization of Cobalt Thin Films Grown by Metal-Organic CVD," Chem. Vap. Depos., vol. 11, no. 5, pp. 235–243, May 2005.

M. Hauschildt, M. Gall, P. Justison, R. Hernandez, M. Herrick, S. Ogawa, P. S. Ho, and E. Zschech, "Large-Scale Statistical Study of Electromigration Early Failure for Cu/low-k Interconnects," AIP Conf. Proc., vol. 945, pp. 66–81, 2007.

Ma, Q.; Guo, H.; Gordon, R. G.; Zaera, F. Chem. Mater. 2011, 23, 3325–3334.

McCrate, J. M.; Ekerdt, J. G. Langmuir 2013, 29, 11868–11875.

N. Deo, M. F. Bain, J. H. Montgomery, and H. S. Gamble, "Study of magnetic properties of thin cobalt films deposited by chemical vapour deposition," J. Mater. Sci. Mater. Electron., vol. 16, no. 7, pp. 387–392, Jul. 2005.

Nicholson, K. T.; Minton, T. K.; Sibener, S. J. J. Phys. Chem. B 2005, 109, 8476–8480.

O. Aubel, C. Hennesthal, M. Hauschildt, A. Beyer, J. Poppe, G. Talut, M. Gall, J. Hahn, J. Boemmels, M. Nopper, and R. Seidel, "Backend-of-Line Reliability Improvement Options for 28nm Node Technologies and Beyond," IEEE, pp. 26–28, 2011.

O. Aubel, J. Hohage, F. Feustel, C. Hennesthal, U. Mayer, A. Preusse, M. Nopper, and M. U. Lehr, "Process options for improving electromigration performance in 32nm technology and beyond," in IEEE: 47th Annual International Reliability Physics Symposium, 2009, pp. 832–836.

O. Aubel, S. Thierbach, R. Seidel, B. Freudenberg, M. A. Meyer, F. Feustel, J. Poppe, M. Nopper, A. Preusse, and C. Zistl, "Comprehensive reliability analysis of CoWP Metal Cap unit processes for high volume production in sub-μm dimensions," pp. 675–676, 2008.

O. Nilsen, O. B. Karlsen, A. Kjekshus, and H. Fjellvåg, "Simulation of growth dynamics in atomic layer deposition. Part I. Amorphous films," Thin Solid Films, vol. 515, no. 11, pp. 4527–4537, Apr. 2007.

O. Nilsen, O. B. Karlsen, A. Kjekshus, and H. Fjellvåg, "Simulation of growth dynamics for nearly epitaxial films," J. Cryst. Growth, vol. 308, no. 2, pp. 366–375, Oct. 2007.

O. Nilsen, O. B. Karlsen, A. Kjekshus, and H. Fjellvåg, "Simulation of growth dynamics in atomic layer deposition. Part II. Polycrystalline films from cubic crystallites," Thin Solid Films, vol. 515, no. 11, pp. 4538–4549, Apr. 2007.

O. Nilsen, O. B. Karlsen, A. Kjekshus, and H. Fjellvåg, "Simulation of growth dynamics in atomic layer deposition. Part III. Polycrystalline films from tetragonal crystallites," Thin Solid Films, vol. 515, no. 11, pp. 4550–4558, Apr. 2007.

O. Nilsen, O. B. Karlsen, A. Kjekshus, and H. Fjellvåg, "Simulation of growth dynamics for nearly epitaxial films," J. Cryst. Growth, vol. 308, no. 2, pp. 366–375, Oct. 2007.

O. Nilsen, O. B. Karlsen, A. Kjekshus, and H. Fjellvåg, "Simulation of growth dynamics in atomic layer deposition. Part I. Amorphous films," Thin Solid Films, vol. 515, no. 11, pp. 4527–4537, Apr. 2007.

P. Moon, V. Dubin, S. Johnston, J. Leu, K. Raol, and C. Wu, "Process Roadmap and Challenges for Metal Barriers," IEEE - IEDM, no. C, pp. 841–844, 2003.

Papageorgiou, N.; Portail, M.; Layet, J. M. Surf. Sci. 2000, 454-456, 462–466.

Papworth, A. J.; Kiely, C. J.; Burden, A. P.; Silva, S. R. P.; Amaratunga, G. A. J. Phys. Rev. B 2000, 62, 12628–12631.

Park, G.-G.; Yang, T.-H.; Yoon, Y.-G.; Lee, W.-Y.; Kim, C.-S. Int. J. Hydrogen Energy 2003, 28, 645–650.

Petrii, O. A. J. Solid State Electrochem. 2008, 12, 609–642.

Prodanov, N. V.; Khomenko, A. V. Surf. Sci. 2010, 604, 730–740.

R. G. Filippi, P.-C. Wang, a. Brendler, K. Chanda, and J. R. Lloyd, "Implications of a threshold failure time and void nucleation on electromigration of copper interconnects," J. Appl. Phys., vol. 107, no. 10, p. 103709, 2010.

R. G. Gordon, H. Kim, and H. Bhandari, "Cobalt Nitride Layers for Copper Interconnects and Methods for Forming Them," US 2008/0254232 A12008.

R. G. Gordon, H. Kim, and H. Bhandari, "Cobalt Nitride Layers for Copper Interconnects and Methods for Forming Them," US 7,973,789 B22011.

Ratsch, C.;Venables, J. A. J. Vac. Sci. Tech. A 2003, 21, S96–S109.

Ritter, R.; Kowarik, G.; Meissl, W.; S€uss, L.; Maunoury, L.; Lebius, H.; Dufour, C.; Toulemonde, M.; Aumayr, F. Nuclear Instrum. Methods Phys. Res., Sect. B 2010, 268, 2897–2900.

S. F. Bent, J. S. Kachian, J. C. F. Rodríguez-Reyes, and A. V Teplyakov, "Tuning the reactivity of semiconductor surfaces by functionalization with amines of different basicity.," Proc. Natl. Acad. Sci. U. S. A., vol. 108, no. 3, pp. 956–60, Jan. 2011.

S. Hofmann, "Profile reconstruction in sputter depth profiling," Thin Solid Films, vol. 398–399, pp. 336–342, Nov. 2001.

S. Hofmann, "Sputter depth profile analysis of interfaces," Reports Prog. Phys., vol. 61, pp. 827–888, 1998.

Serin, V.; Brydson, R.; Scott, A.; Kihn, Y.; Abidate, O.; Maquin, B.; Derre, A. Carbon. 2000, 38, 547–554.

Service, R. F. Science 2002, 296, 64–66.

T. D. Elko-Hansen, A. D. Dolocan, and J. G. Ekerdt, “Interdiffusion and diffusive stabilization of cobalt by copper during atomic layer deposition from bis (N- tert-butyl- N ’ -ethylpropionamidinato) cobalt (II),” Rev., pp. 1–13, 2014.

T. D. M. Elko-Hansen and J. G. Ekerdt, “XPS investigation of the atomic layer deposition half reactions of bis (N-tert-butyl-N ’ -ethylpropionamidinato) cobalt (II).” Austin, 2014.

T. Kirimura, K. Croes, Y. K. Siew, K. Vanstreels, P. Czarnecki, Z. El-mekki, M. H. Van Der Veen, D. Dictus, A. Yoon, A. Kolics, J. Bömmels, and Z. Tőkei, “Void nucleation and growth during electromigration in 30 nm wide Cu lines : Impact of different interfaces on failure mode,” IEEE, 2013.

T. Yoda and H. Miyajima, “Advanced BEOL Technology Overview,” in Advanced Nanoscale ULSI Interconnects: Fundamentals and Applications, 2009, pp. 275–298.

Venables, J. A.; Giordano, L.; Harding, J. H. J. Phys.: Condens. Matter 2006, 18, S411–S427.

Wang, T.; Ekerdt, J. G. Chem. Mater. 2009, 21, 3096–3101.

Wedding, J. B.; Wang, G.; Lu, T.-M. Surf. Sci. 2002, 504, 28–36.

Wu, W.; Yuan, J. S. Solid. State. Electron. 2011, 45, 2011–2016.

Yang, C.-C.; Flaitz, P.; Wang, P.-C.; Chen, F.; Edelstein, D. IEEE Electron Device Lett. 2010, 31, 728–730.

Yang, D.-Q.; Sacher, E. J. Phys. Chem. C 2008, 112, 4075–4082.

Yang, D.-Q.; Sacher, E. Surf. Sci. 2002, 516, 43–55.

Li, Z.; Lee, D. K.; Coulter, M.; Rodriguez, L. N. J.; and Gordon, R. G. “Synthesis and characterization of volatile liquid cobalt amidinates.,” Dalton Trans., no. 19, pp. 2592–2597, May 2008.

Li, Z.; Barry, S. T.; and Gordon, R. G. “Synthesis and characterization of copper(I) amidinates as precursors for atomic layer deposition (ALD) of copper metal.,” Inorg. Chem., vol. 44, no. 6, pp. 1728–35, Mar. 2005.

Wu, Z.-J.; Cao, L.; Im, J.; Lee, K.-D.; and Ho, P. S. “Critical initial void growth for electromigration: Stress modeling and multi-link statistics for Cu/low-k interconnects,” 2013 IEEE Int. Interconnect Technol. Conf. - IITC, pp. 1–3, Jun. 2013.

Zhou, Y.;Pasquarelli,R.;Holme,T.;Berry, J.;Ginley,D.;O’Hayre, R. J. Mater. Chem. 2009, 19, 7830.

Zhu, Y.-J.; Schnieders, A.; Alexander, J. D.; Beebe, T. P., Jr. Langmuir 2002, 18, 5728–5733.

Zhuravlev, L. T. Colloids Surfaces A Physicochem. Eng. Asp. 2000, 173, 1–38.

Vita

Tyler Don-Michel Elko-Hansen was born and raised in Colorado. He attended the University of Colorado at Boulder from 2004 – 2009 at which he attained a Bachelor of Science degree in Chemical Engineering with a minor in Germanic Studies. During his undergraduate studies, Tyler performed and supported research efforts at several institutions. During the first year of his undergraduate studies, he supported the research of Mei Hong in the Richard Noble group investigating *Zeolite Membranes for Gas Separation.* Tyler subsequently worked for six months at the BMW Research and Development center in Munich, Germany on the development of *Alternative Hydrogen Storage Methods.* Finally, Tyler spent one and one-half years working at the National Renewable Energy Laboratory in Golden, CO researching *Carbonaceous Hydrogen Storage Materials*. In the Fall of 2009, Tyler began his PhD studies at The University of Texas at Austin with his adviser Dr. John G. Ekerdt.

Permanent email address: tyler.elkohansen@gmail.com

This dissertation was typed by Tyler Don-Michel Elko-Hansen.